Supplementary Information for:

Pedigree-based and phylogenetic methods support surprising patterns of mutation rate and spectrum in the gray mouse lemur

C. Ryan Campbell[1,2], George P. Tiley[1], Jelmer W. Poelstra[1], Kelsie E. Hunnicutt[1,†], Peter A. Larsen[1,‡], Hui-Jie Lee[3], Jeffrey L. Thorne[4], Mario dos Reis[5], Anne D. Yoder[1*]

[1]Department of Biology, Duke University, Durham, NC 27708, USA

[2]Department of Evolutionary Anthropology, Duke University, Durham, NC 27708, USA

[3]Department of Biostatistics and Bioinformatics, Duke University, Durham, NC 27708, USA

[4]Bioinformatics Research Center, North Carolina State University, Raleigh, NC 27695, USA

[5]School of Biological and Chemical Sciences, Queen Mary University of London, Mile End Road, London E1 4NS, UK

[†]Present address: Department of Biological Sciences, University of Denver, Denver, CO 80208

[‡]Present address: Department of Veterinary and Biomedical Sciences, University of Minnesota, St. Paul, MN 55108

*Author for Correspondence: anne.yoder@duke.edu

Contents

Variant Calling's Effect on *de novo* Mutation Rate Estimation

An attempt to, given a duplicate sample providing a known variant call error rate, quantify the effects of incorrect variant calls on the estimation of de novo mutations.

Our knowns are as follows, the number of sites in the genome with sufficient coverage to make *de novo* calls (sites, s), the number of variants (variants, v) in the entire pedigree (v_{ped}), the mother's sample (v_m), the father's sample (v_f), and the offspring sample (v_o). Also the number of unique variants (unique variants, w) in the entire pedigree (w_p), the mother's sample (w_m), the father's sample (w_f), and the offspring sample (w_o). We also know the error rate of the replicated sample, presented here as a fraction of variants called (called error rate, c). This is an average rate of variants that are present in one replicate and absent in the other. We also assume the transmission probability of any given site is 0.5 (transmission probability, t). Finally we'll add a single unknown variable (e), which is the fraction of erroneous variant calls that are false negatives. This variable ranges from 0 to 1, with 1 representing the scenario where all erroneous calls are false negatives. We have no reason to expect that this fraction differs across the replicates. This variable will allow us to explore a range of possible error effects. It will also allow us to be conservative (taking the value of e that yields the most error) when reaching a final conclusion regarding error rates. The probability that a *de novo* mutation call is a false positive is simply the probability of a false positive variant within the offspring that is not already a variant in the pedigree or a parental false negative at a site that is unique to the individual and transmitted.

$$P(\mu_{f+}) = P(unique\ offspring\ false\ positive) + P(shared\ paternal\ false\ negative) + P(shared\ maternal\ false\ negative) \tag{1}$$

$$P(unique\ offspring\ false\ positive) = c * e * \frac{w_o}{v_o} \tag{2}$$

$$P(shared\ paternal\ false\ negative) = \frac{c * v_f}{s} * (1 - e) * \frac{w_o}{v_o} \tag{3}$$

$$P(shared\ maternal\ false\ negative) = \frac{c * v_m}{s} * (1 - e) * \frac{w_o}{v_o} \tag{4}$$

So, substituting the these into the original equation:

$$P(\mu_{f+}) = c * e * \frac{w_o}{v_o} + \frac{c * v_m}{s} * (1 - e) * \frac{w_o}{v_o} + \frac{c * v_f}{s} * (1 - e) * \frac{w_o}{v_o} \tag{5}$$

$$P(\mu_{f+}) = \frac{c * w_o}{v_o} * (e + \frac{v_f * v_m * (1 - e)}{s}) \tag{6}$$

The probability that a genomic site with sufficient coverage is an uncalled false negative *de novo* mutation call is essentially the converse of the false positive. It is the probability of a false negative within the offspring that is not already a variant in the pedigree or a parental false positive at a site that is unique to the individual and transmitted.

$$P(\mu_{f-}) = P(unique\ offspring\ false\ negative) + 2 * P(shared\ parental\ false\ positive) \tag{7}$$

$$P(unique\ offspring\ false\ negative) = (1 - \frac{w_o}{s}) * \frac{c}{s} * (1 - e) \tag{8}$$

$$P(shared\ parental\ false\ positive) = c * e * \frac{w_o}{s} \tag{9}$$

So, substituting the these into the original equation:

$$P(\mu_{f-}) = (1 - \frac{w_o}{s}) * \frac{c}{s} * (1 - e) + c * e * \frac{w_o}{s} + c * e * \frac{w_o}{s} \tag{10}$$

$$P(\mu_{f-}) = \frac{c}{s} * ((1 - \frac{w_o}{s}) * (1 - e) + 2 * w_o * e) \tag{11}$$

Using as known values (where for sets of variants w_o is the average of w_{o1} and w_{o2}):

$$c = 0.021$$

$$e = 0.5$$

$$s = 2.074 * 10^9$$

$$\mu_{dn} = 92$$

$$v_{o1} = 29,574$$

$$v_{o2} = 31,444$$

$$v_m = 28,598$$

$$v_f = 30,997$$

$$w_{o1} = 1,729$$

$$w_{o2} = 1,522$$

$$w_m = 1,200$$

$$w_f = 2,085$$

The probabilites of false negative and false positives are as follows:

$$P(\mu_{f+}) = 3.72 * 10^{-2}$$

$$P(\mu_{f-}) = 1.67 * 10^{-8}$$

Given 92 *de novo* mutations from 2,074,177,339 sites of sufficient coverage, we expect:

$$E(\mu_{f+}) = \mu_{dn} * P(\mu_{f+})$$

$$E(\mu_{f+}) = 3.43$$

$$E(\mu_{f-}) = s * P(\mu_{f-})$$

$$E(\mu_{f-}) = 34.5$$

de novo Mutation Rate Credible Intervals

To estimate the credible interval of the de novo mutation rate of the Gray Mouse Lemur, we used a Bayesian method and assumed mutations follow a poisson distribution.

We set the total number of *de novo* mutations in a single individual to λ, and assume that the mutations inhereted from each parent have a Poisson distribution, then the total number of mutations inherited also follows a Poisson distribution. Let $\mathrm{x_i}$ be the total number of mutations observed in an individual, and suppose we observe mutations in n individuals. We can use a Bayesian method to estimate the credible interval of the mutation rate, λ. Note that the gamma distribution is the conjugate prior of the Poisson, and thus we use a gamma prior on λ with parameters α (shape) and β (rate). The posterior distribution is:

$$f_\lambda(\lambda|x_1,...,x_\mathrm{n}) \propto \lambda^{\alpha-1}e^{-\beta\lambda} \times \prod_{i=1}^{n} \frac{\lambda^{x_i}e^{-\lambda}}{x_i!} \tag{1}$$

$$\propto \lambda^{\alpha+\sum x_i-1}e^{-(\beta+n)\lambda} \tag{2}$$

Thus, the posterior of λ is a gamma distribution with parameters $\alpha + \sum x_\mathrm{i}$ (shape) and $\beta + n$ (rate). Our knowns are the number of mutations observed in each individual ($\mathrm{x_1} = 65.4$ $\mathrm{x_2} = 57.7$). Let the prior on λ be represented by a gamma distribution with shape parameters $\alpha = 2$ and $\beta = 0.02$. This is a diffuse prior with mean $\alpha/\beta = 100$ mutations. Thus the estimate of λ is gamma distributed with shape $2 + 65.4 + 57.7 = 125.03$ and rate $0.02 + 2 = 2.02$. Thus the posterior mean is $\widetilde{\lambda} = 62.5$, posterior standard deviation $\widetilde{s} = \sqrt{125.03}/2.02 = 5.54$. Note this estimate of λ is given as mutations per genome. To get the rate per nucleotide site, we simply divide by the callable, diploid genome size, g. For example, assuming this is $g = 2 * 2.04 \times 10^{-9}$ in mouse lemurs, we get $\widetilde{\lambda} = 1.52 \times 10^{-8}$ and $s = 1.36 \times 10^{-9}$, The 95% credibility interval for the estimate between 52.9 and 73.1 mutations per genome, or between 1.28×10^{-8} and 1.78×10^{-8} mutations per nucleotide site.

de novo Mutation Rate Calculation

To accurately estimate the de novo mutation rate of the Gray Mouse Lemur, we counted mutations in a family of four animals, assessed callable sites, accounted for false positive and false negative calls from sequencing data, and combined these values into a weighted average estimate of the final mutation rate.

Our knowns are the size of the mouse lemur genome, g, broken down into autosomes, g_a, and the X chromosome, g_x, the proportion of autosomes, g_{ca}, and the X chromosome, g_{cx}, on which we were able to identify a mutation, also known as the callable sites. We know the total number of mutations found on autosomes in each offspring, m_{1a} and m_{2a}, and on the X chromosome in each offspring, m_{1x} and m_{2x}.

Finally, we are adjusting for errors in variant calling process, by accounting for the rate at which false positives are expected per called mutation, f_p, and the rate at which false negatives are expected per evaluated site, f_n.

The basic calculation for mutation rate is the number of mutations per callable site multiplied by the number of haplotypes measured (2 per individual measured):

$$\frac{m}{n \cdot g_c} \tag{1}$$

To adjust mutation count for false positives and negatives, we reduced the raw count by the fraction of expected false positives and add in the expected false negatives per callable site:

$$m \cdot (1 - f_p) + f_n \cdot g_c \tag{2}$$

The final rate is an average of the rate in autosomes and the X chromosome, weighted by their relative propotions in the genome of the gray mouse lemur:

$$\frac{g_a}{g} \cdot \frac{m_a}{n \cdot g_{ca}} + \frac{g_x}{g} \cdot \frac{m_x}{n \cdot g_{cx}} \tag{3}$$

Combining all of the above we arrive at the final equation for mutation rate in this study, in which we tested 4 autosomes (2 individuals) and 3 X chromosomes (1 male and 1 female).

$$\frac{g_a}{g} \cdot \frac{(m_{1a} + m_{2a}) \cdot (1 - f_p) + f_n \cdot g_{ca}}{4 \cdot g_{ca}} + \frac{g_x}{g} \cdot \frac{(m_{1x} + m_{2x}) \cdot (1 - f_p) + f_n \cdot g_{cx}}{3 \cdot g_{cx}} \tag{4}$$

Supplementary Figures

Figure S1 – Pedigree of all mouse lemur individuals. The focal quartet used for mutation rate estimation is colored in blue. Names of sequenced individuals and SRA identifiers are given. Poblano has two SRA identifiers that correspond to the two separate libraries.

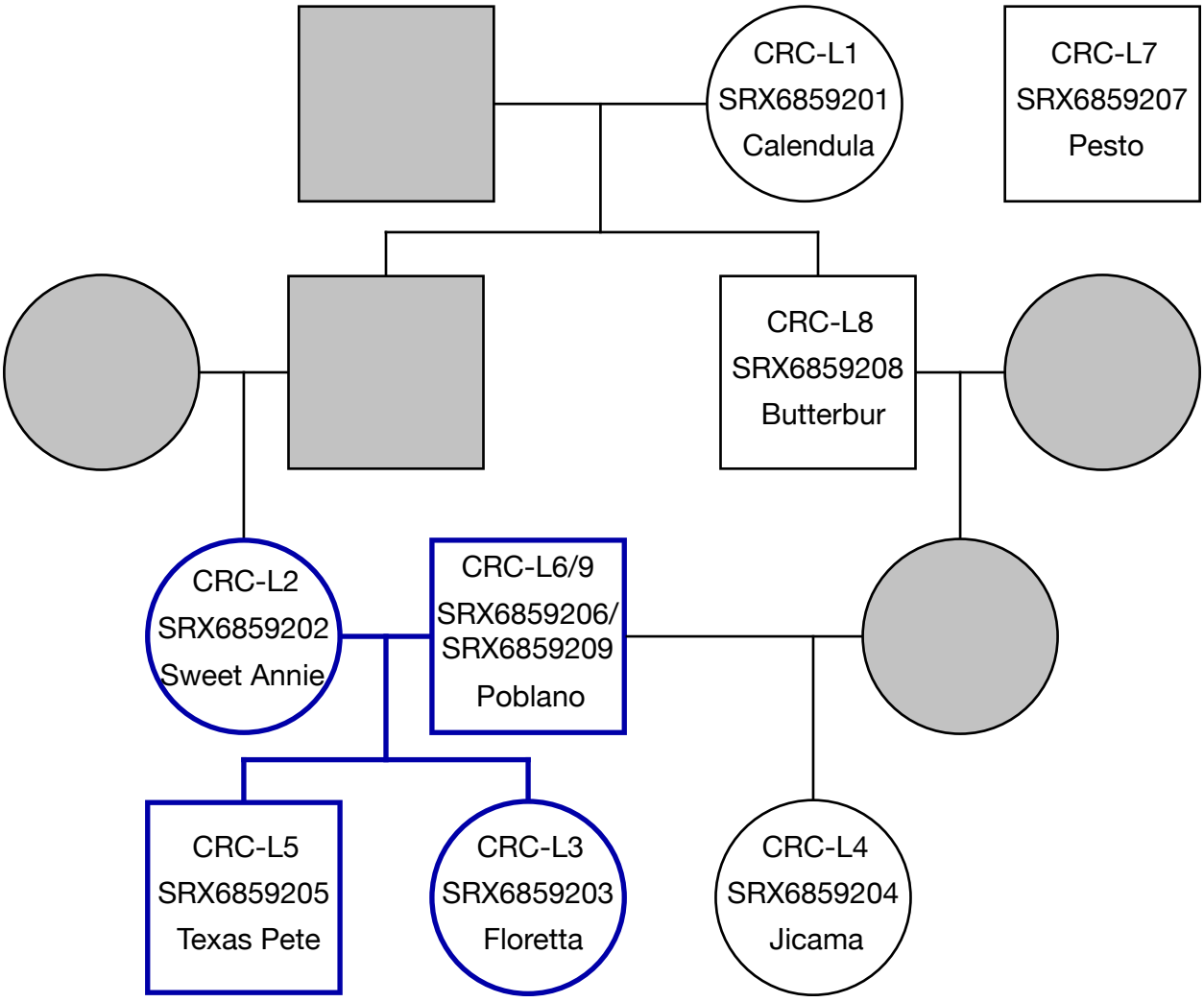

Figure S2 – Allele Balance and Coverage Distribution. 92 mutations were called by DeNovoGear. 15 mutations were excluded when increasing the allele balance filter from 80/20 to 70/30.

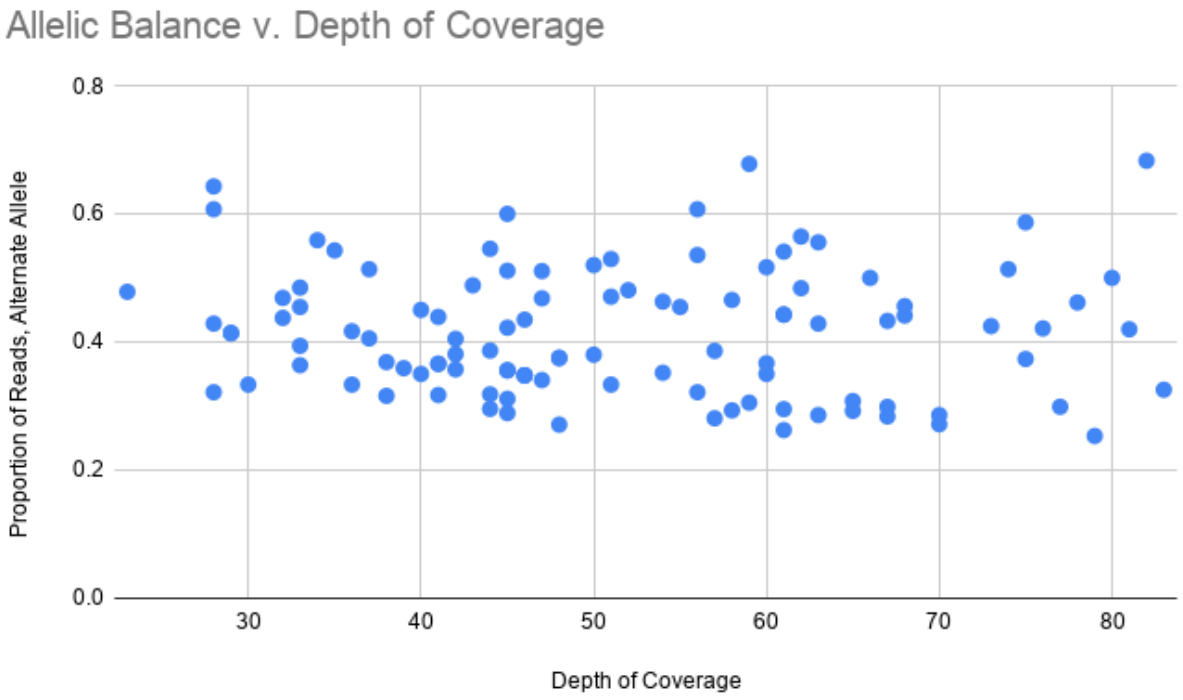

Figure S3 – Mutation 41 at position 43233178 of Chromosome 11 in Texas Pete. Exemplar low-coverage mutation at 33x in the offspring. The 75 bases up and downstream were visualized in IGV.

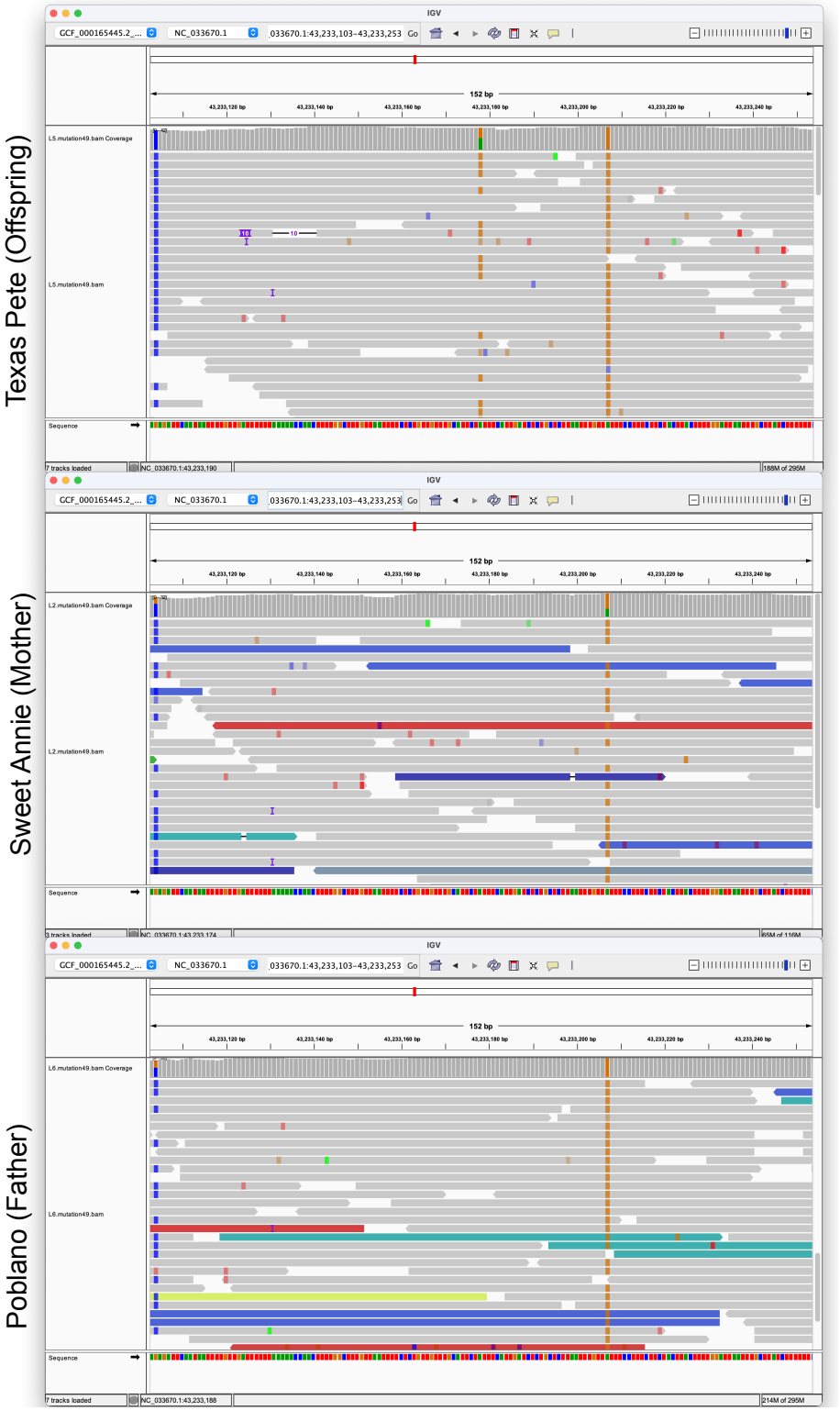

Figure S4 – Mutation 22 at position 86364512 of Chromosome 6 in Texas Pete. Exemplar medium-depth mutation at 41x in the offspring. The 75 bases up and downstream were visualized in IGV.

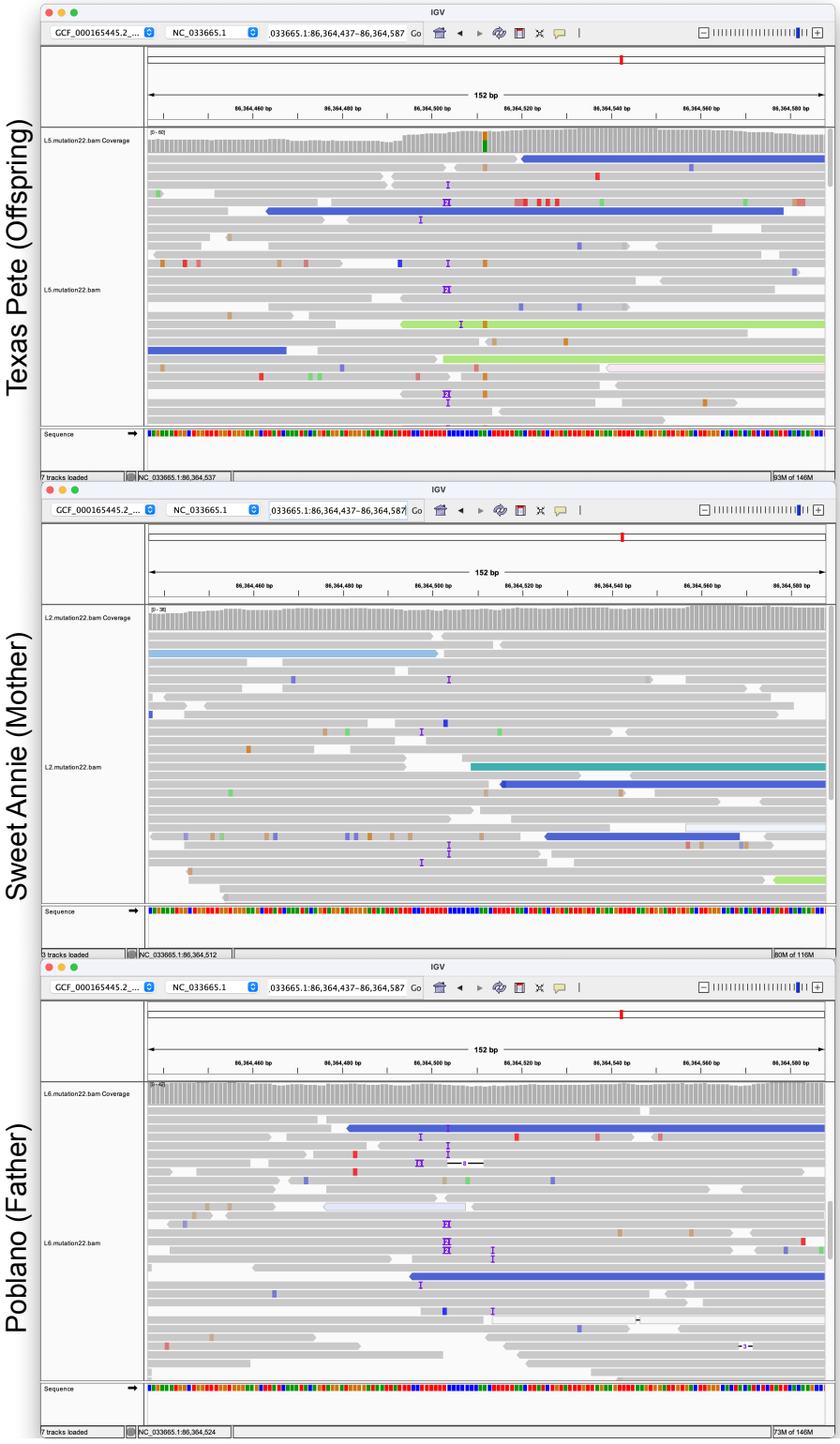

Figure S5 – Mutation 29 at position 38462452 of Chromosome 9 in Floretta. Exemplar medium-depth mutation at 43x in the offspring. The 75 bases up and downstream were visualized in IGV.

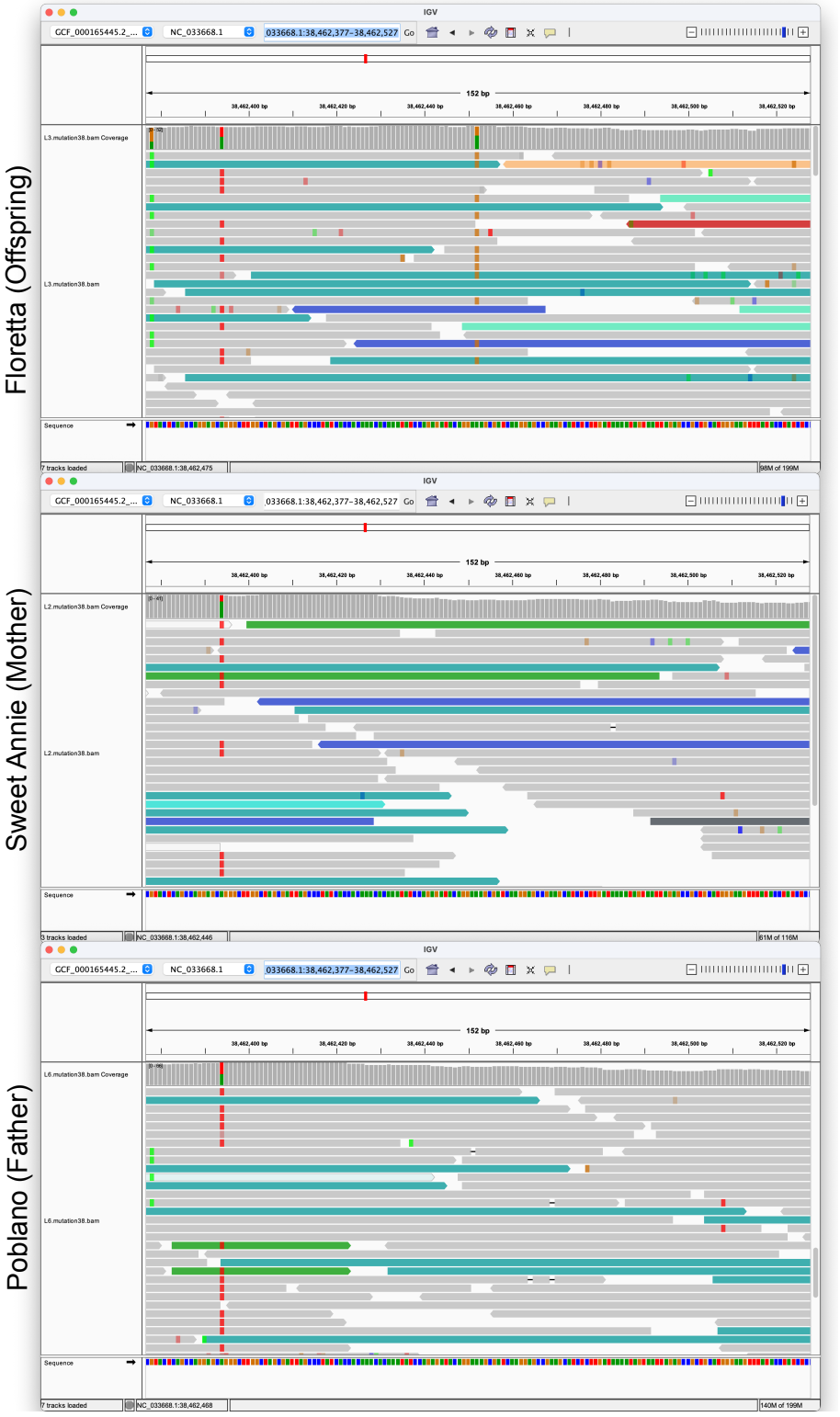

Figure S6 – Mutation 72 at position 55021305 of Chromosome 18 in Texas Pete. Exemplar high-depth mutation at 73x in the offspring. The 75 bases up and downstream were visualized in IGV.

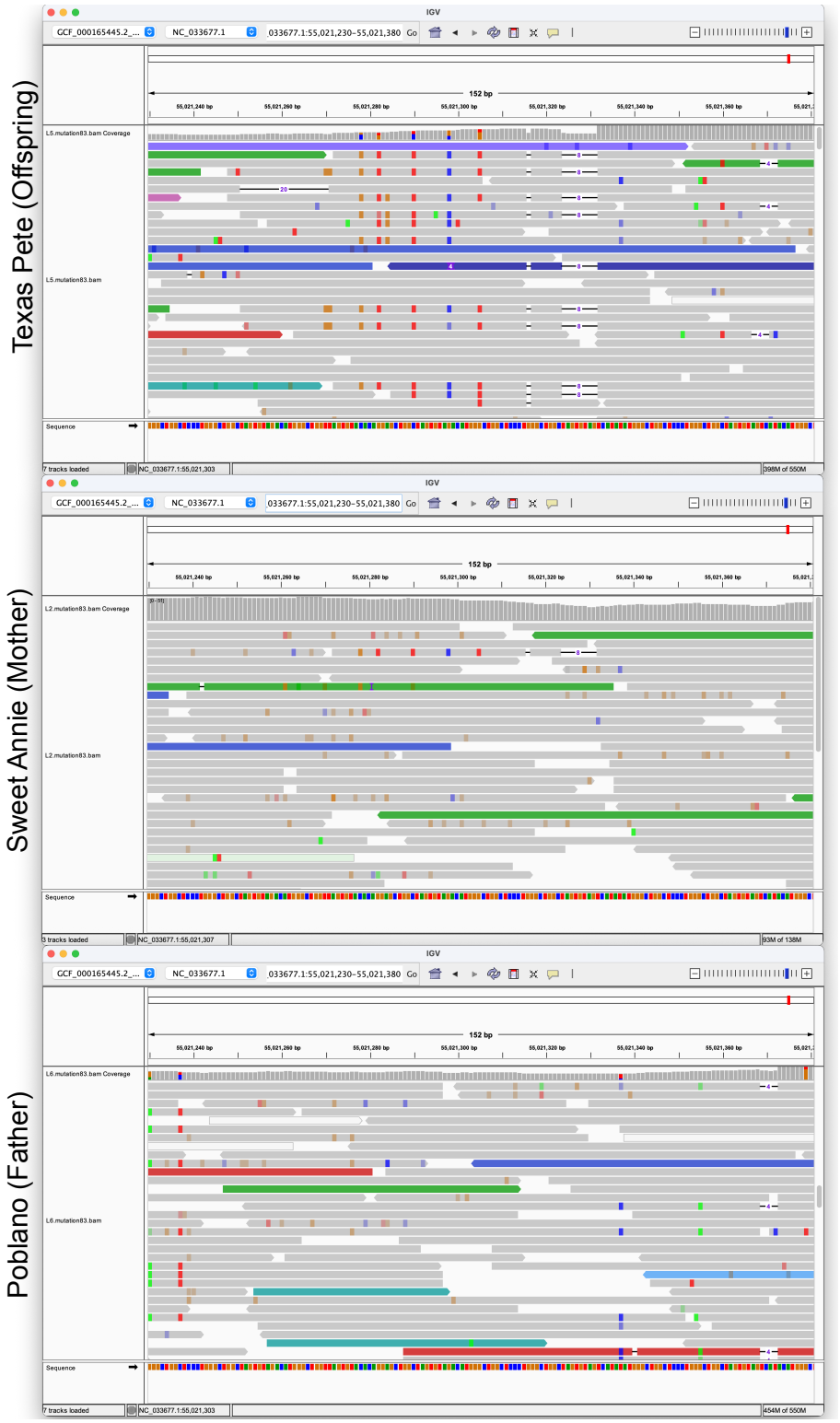

Figure S7 – Effect of assumptions about the proportion of false positives and negatives in the technical replicate on mutation rate. The x-axis is *e*, the proportion of errors between technical replicates that are false negatives. An assumption of *e* = 0.5 was used for or mutation rate calculation, but this can be greatly affected by assuming more or less errors are due to false negatives in one of the replicates. The red line are false positives, blue line is false negatives, and purple is the net change in the number of mutations.

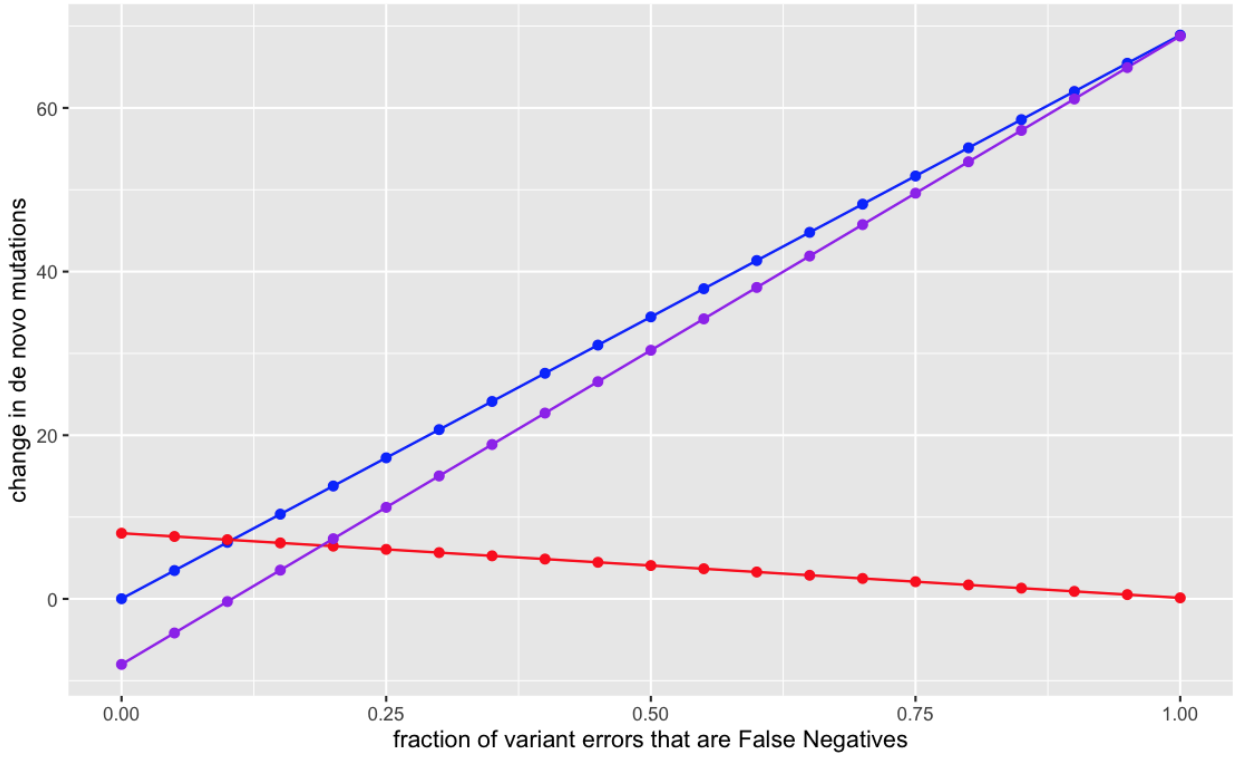

Figure S8 – Key to Clock Model Parameters. Subsequent figures will adopt these symbols for parameters to facilitate visualization. All branches have independent but autocorrelated substitution rates (μ) and node heights (*t*) based on calibration densities in Table S1.

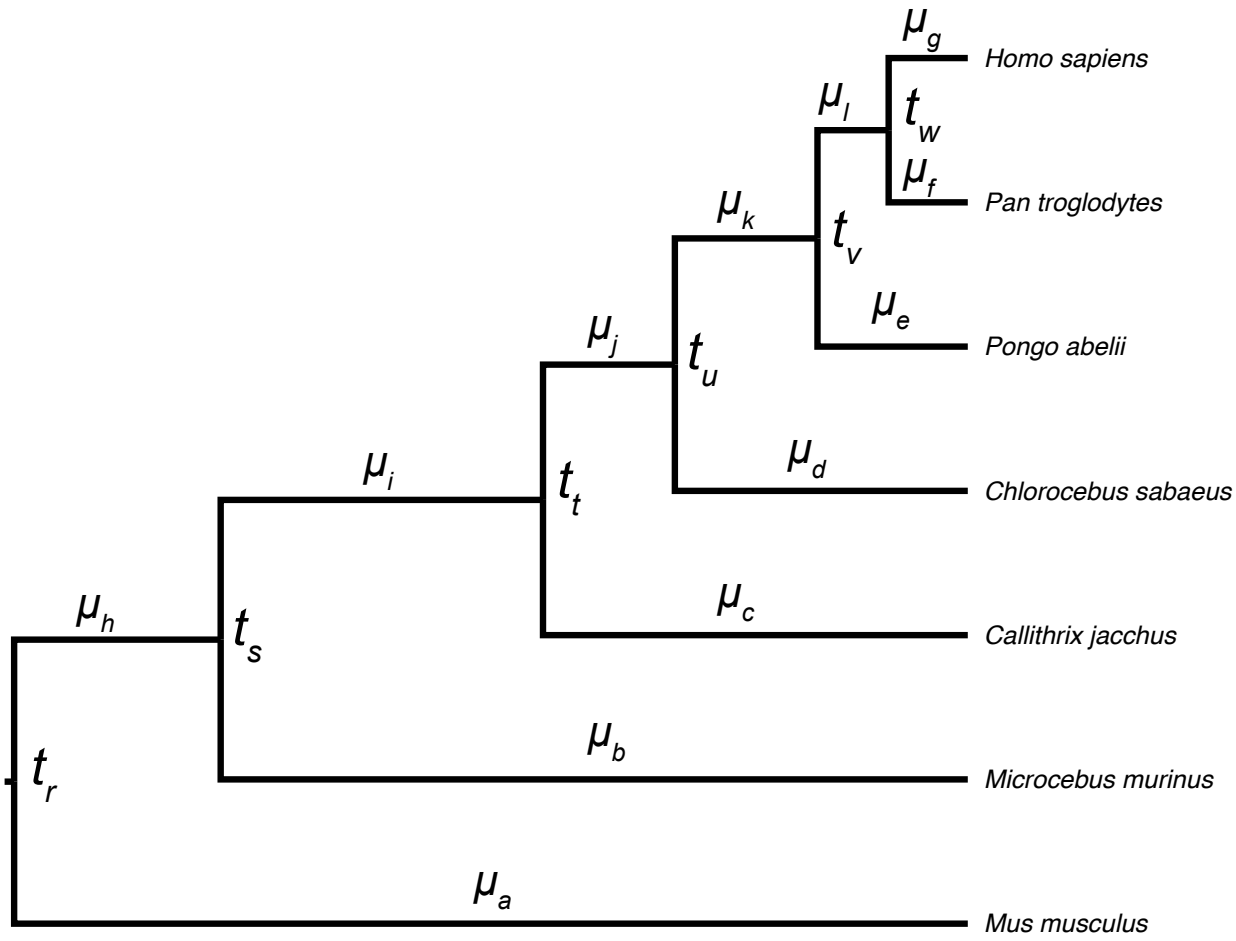

Figure S9 – Convergence of Posteriors for Replicate 1 without Partitioning by Substitution Type. Chains 1 and 2 were combined and are shown in red while chains 3 and 4 are shown in blue. Overlaps of posterior distributions are thus shown in purple.

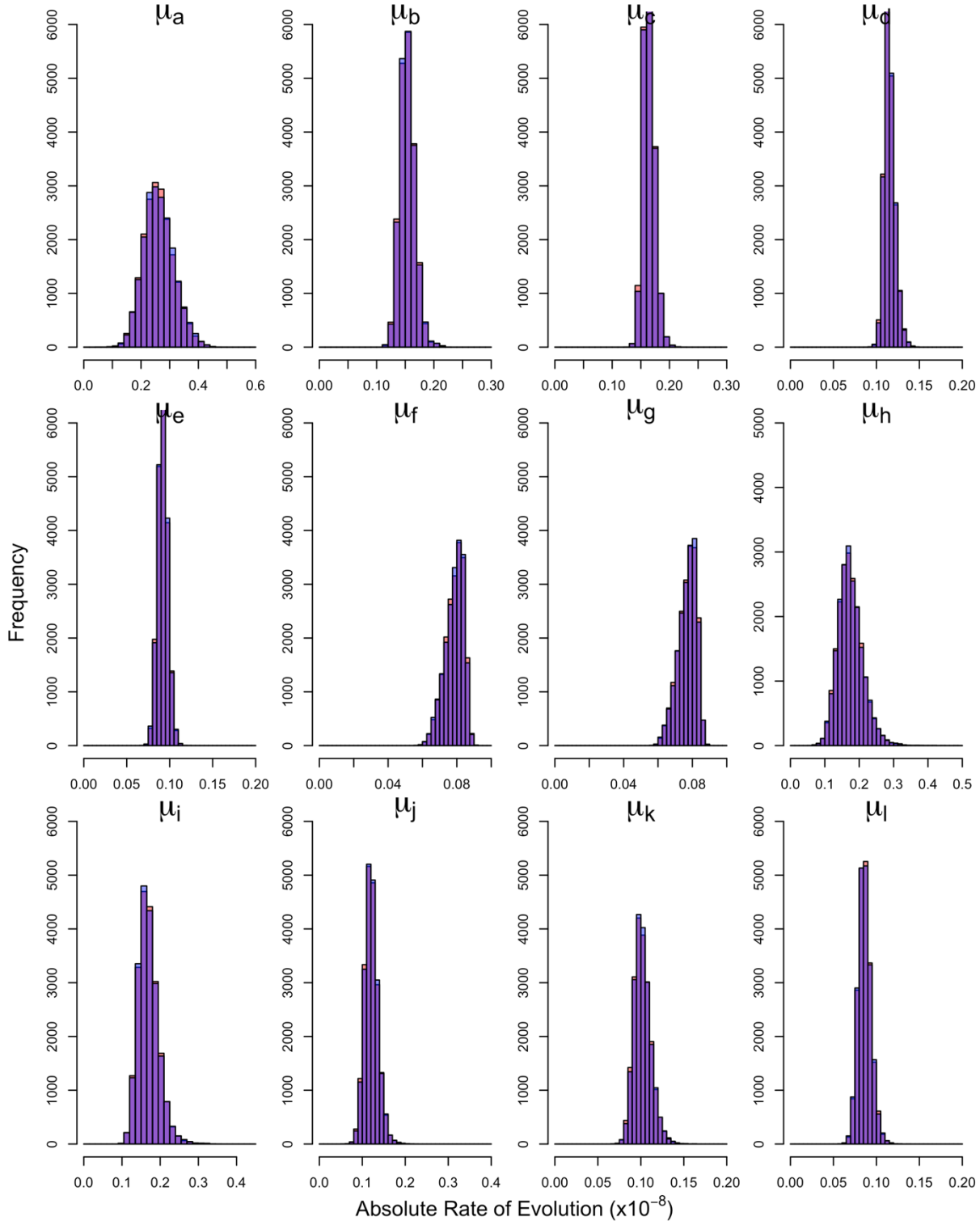

Figure S10 – Convergence of Posteriors for Replicate 2 without Partitioning by Substitution Type. Chains 1 and 2 were combined and are shown in red while chains 3 and 4 are shown in blue. Overlaps of posterior distributions are thus shown in purple.

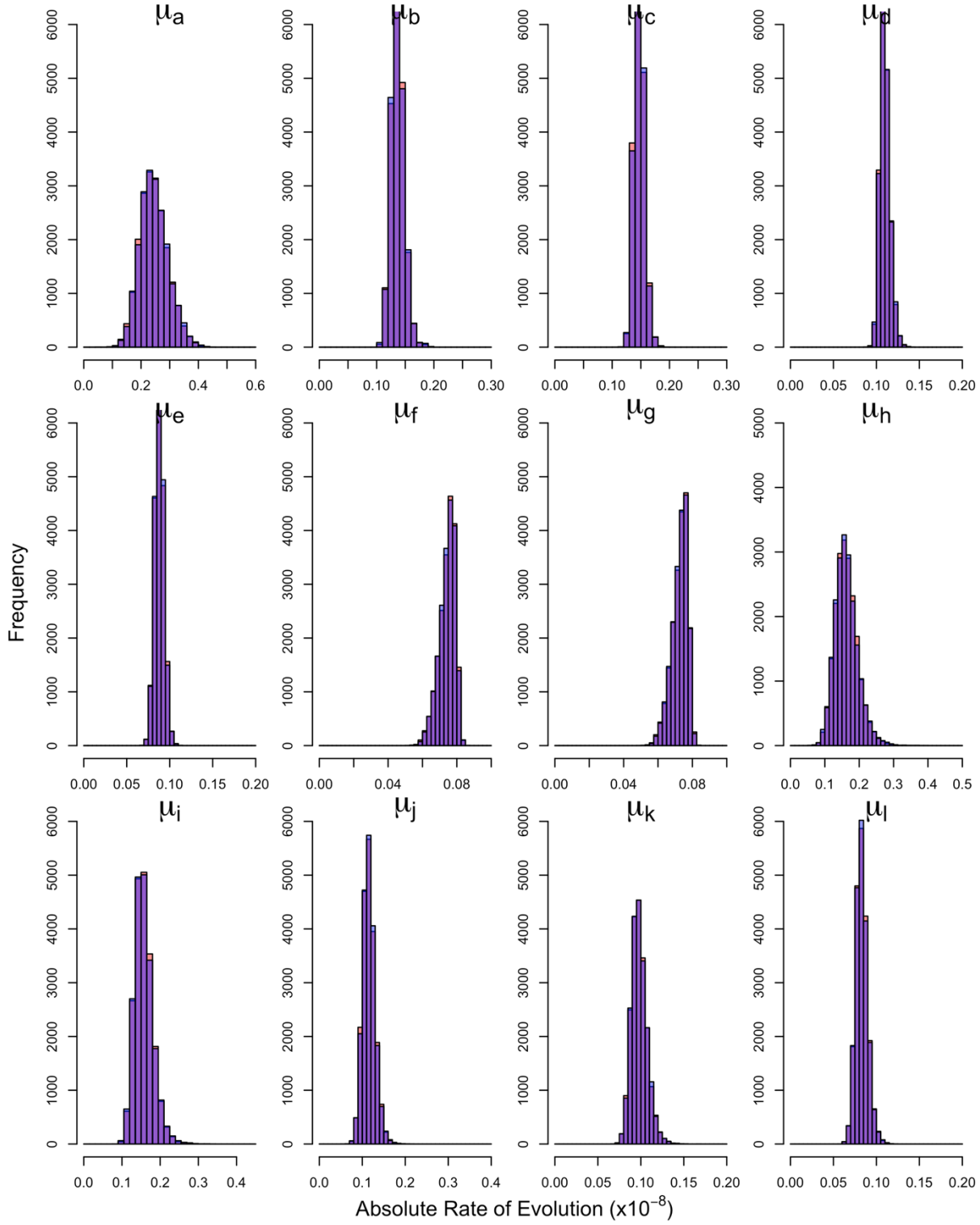

Figure S11 – Convergence of Posteriors for Replicate 3 without Partitioning by Substitution Type. Chains 1 and 2 were combined and are shown in red while chains 3 and 4 are shown in blue. Overlaps of posterior distributions are thus shown in purple.

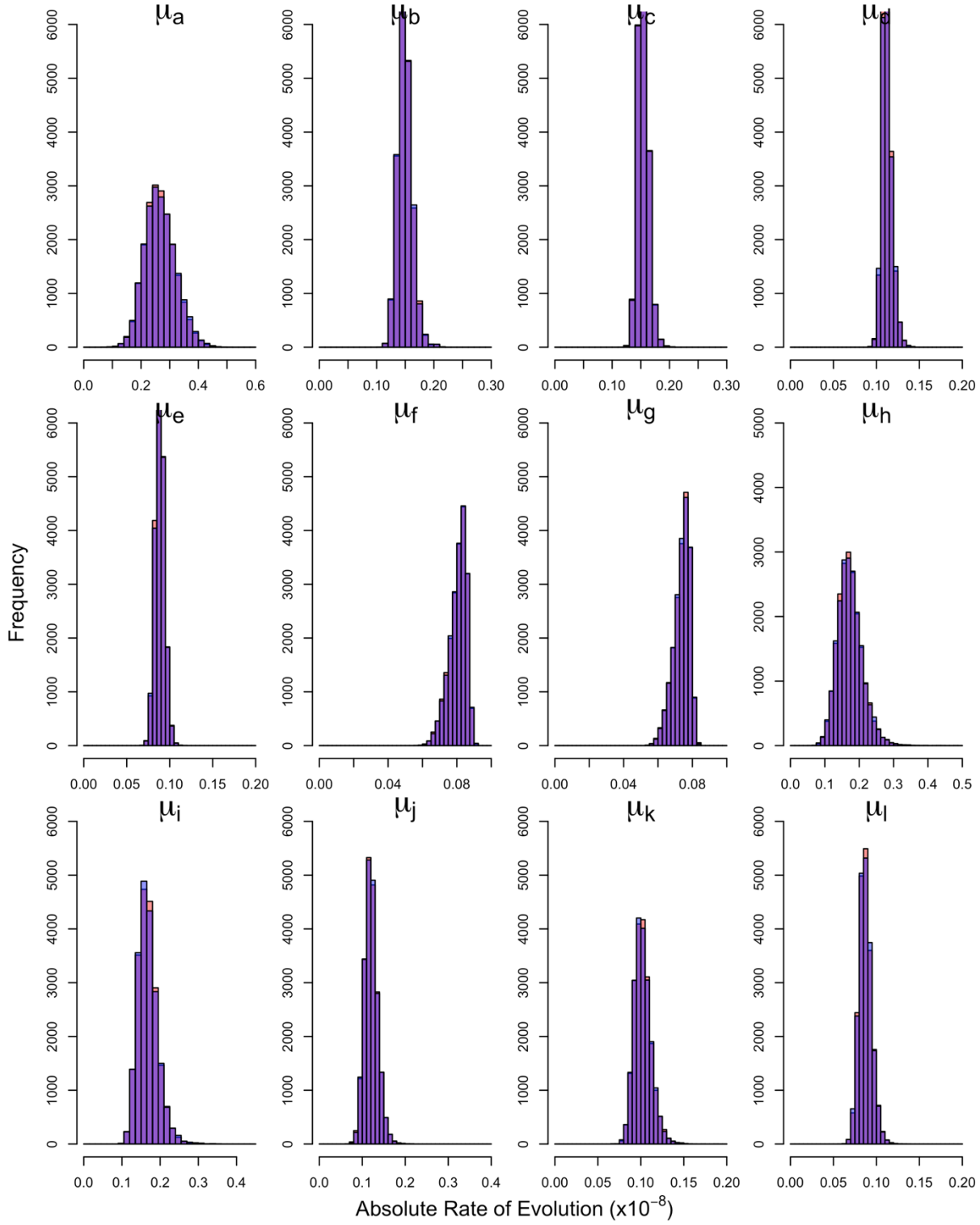

Figure S12 – Convergence of Posteriors for Replicate 4 without Partitioning by Substitution Type. Chains 1 and 2 were combined and are shown in red while chains 3 and 4 are shown in blue. Overlaps of posterior distributions are thus shown in purple.

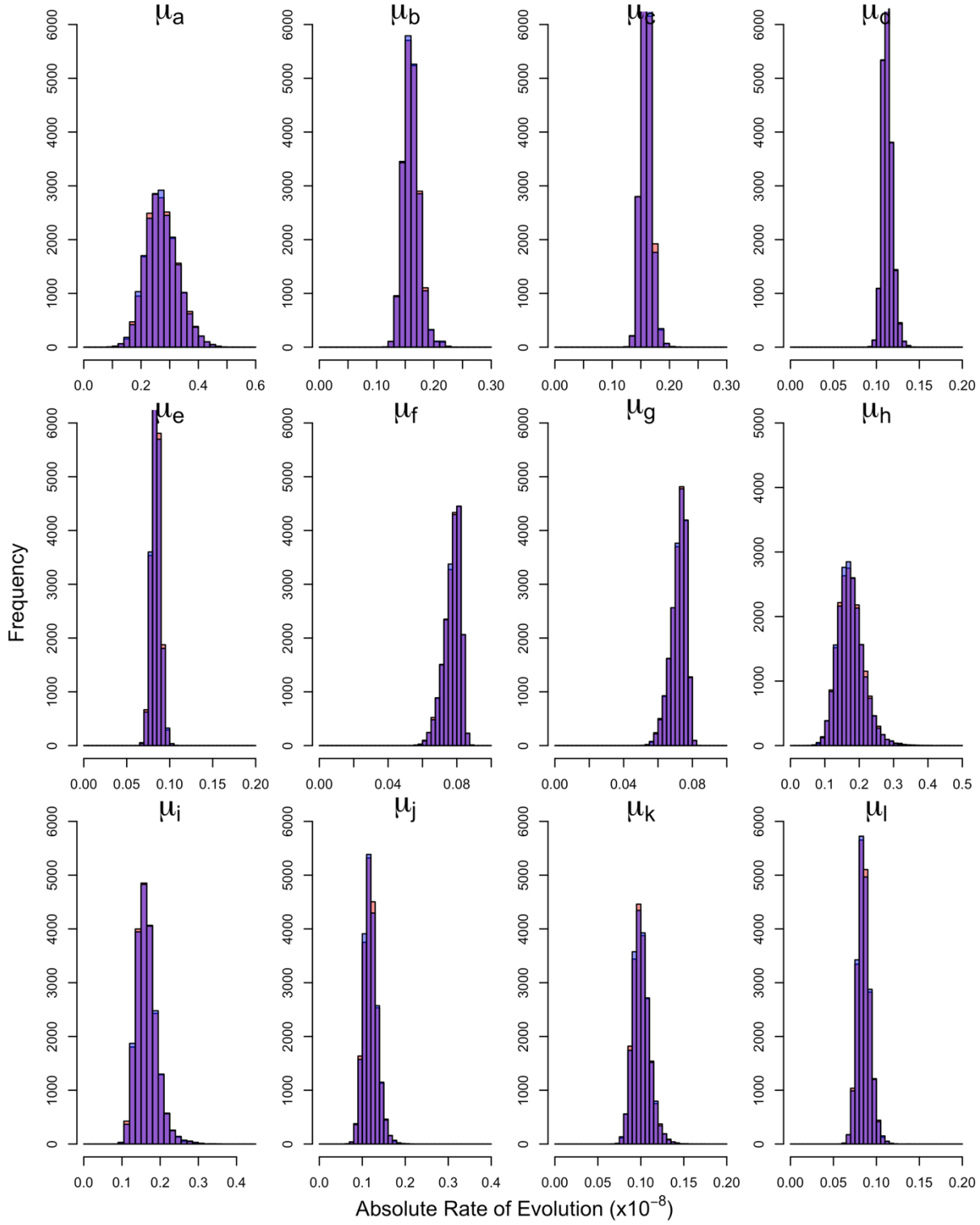

Figure S13 – Convergence of Posteriors for Replicate 5 without Partitioning by Substitution Type. Chains 1 and 2 were combined and are shown in red while chains 3 and 4 are shown in blue. Overlaps of posterior distributions are thus shown in purple.

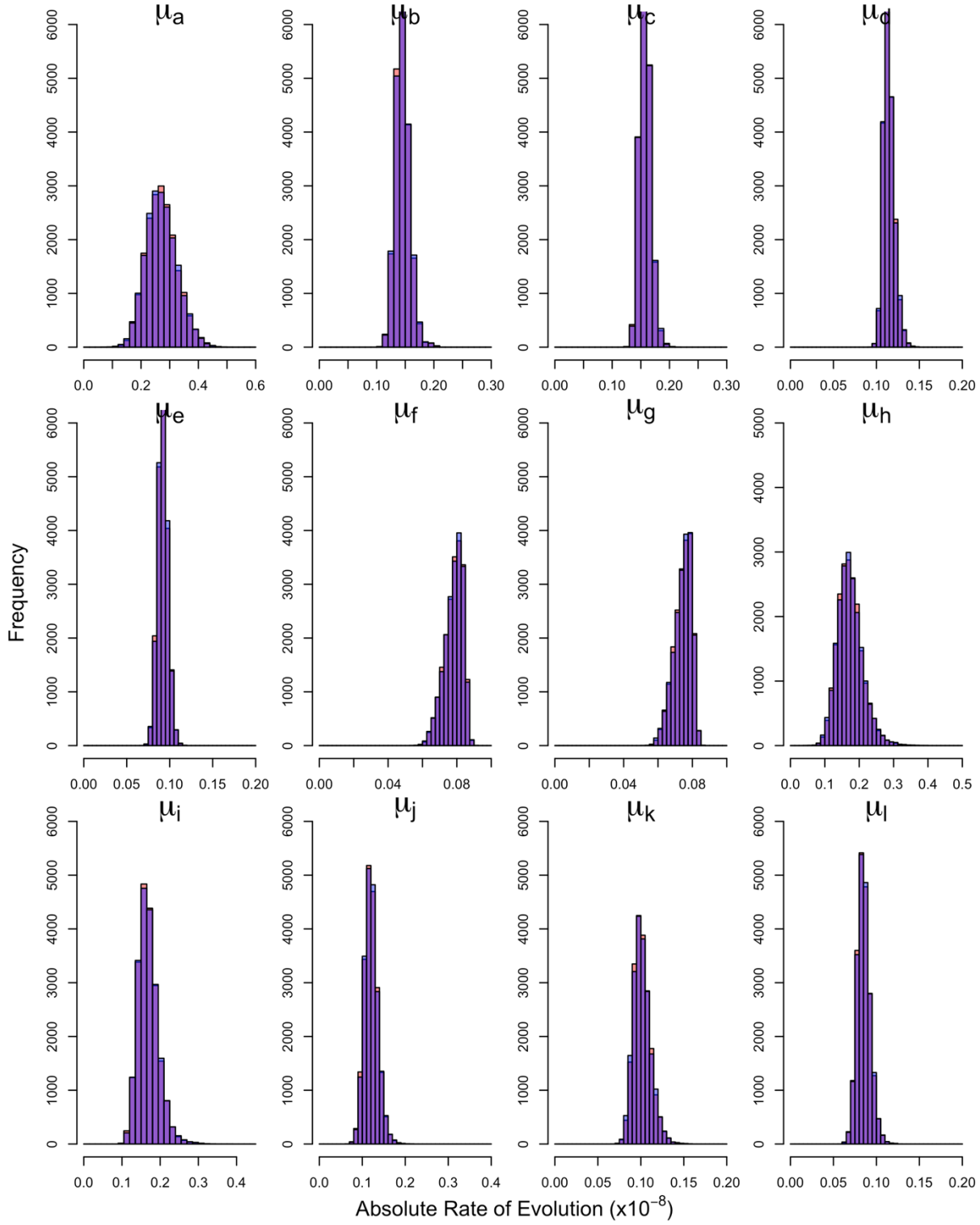

Figure S14 – Convergence of Posteriors for Replicate 6 without Partitioning by Substitution Type. Chains 1 and 2 were combined and are shown in red while chains 3 and 4 are shown in blue. Overlaps of posterior distributions are thus shown in purple.

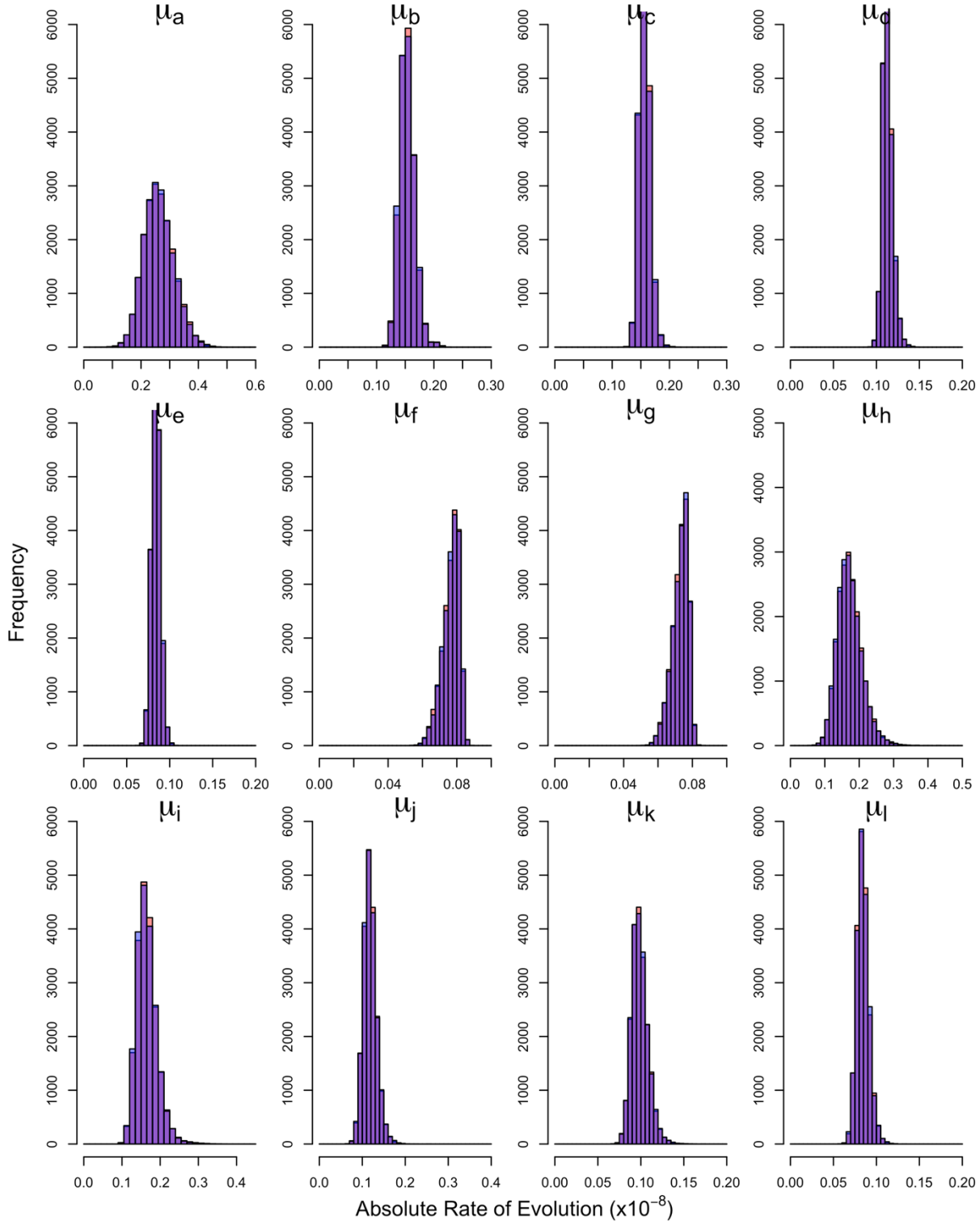

Figure S15 – Convergence of Posteriors for Replicate 7 without Partitioning by Substitution Type. Chains 1 and 2 were combined and are shown in red while chains 3 and 4 are shown in blue. Overlaps of posterior distributions are thus shown in purple.

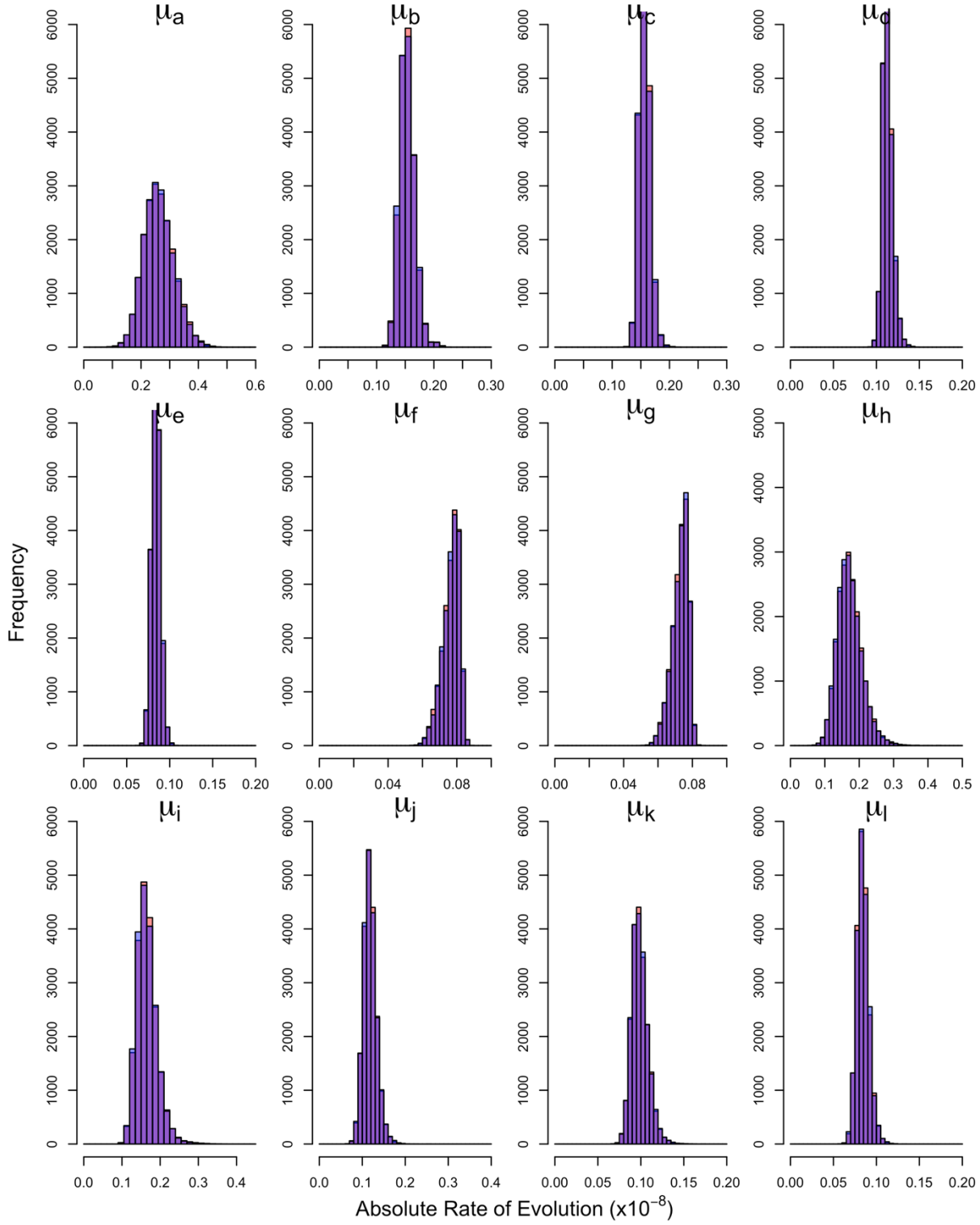

Figure S16 – Convergence of Posteriors for Replicate 8 without Partitioning by Substitution Type. Chains 1 and 2 were combined and are shown in red while chains 3 and 4 are shown in blue. Overlaps of posterior distributions are thus shown in purple.

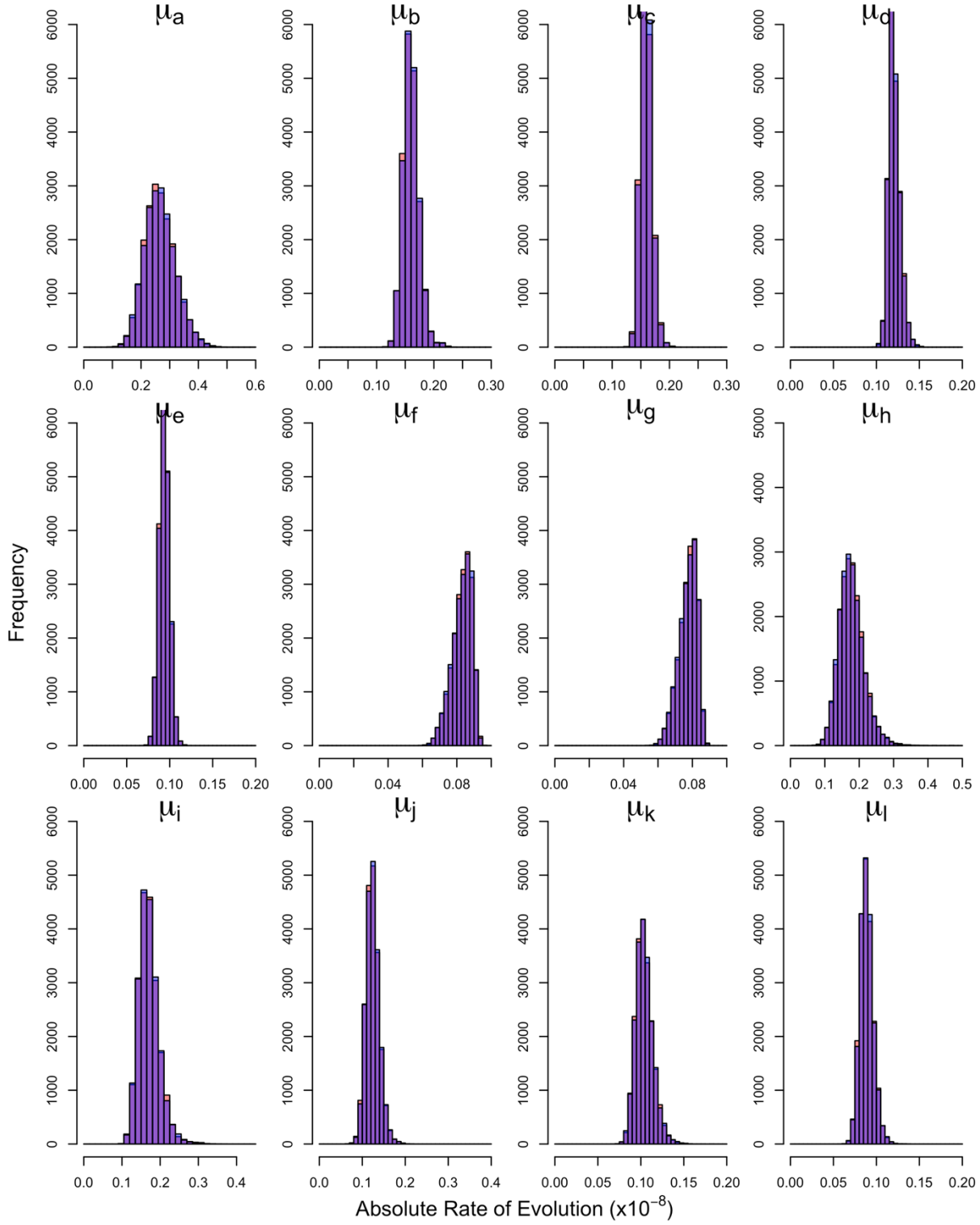

Figure S17 – Convergence of Posteriors for Replicate 9 without Partitioning by Substitution Type. Chains 1 and 2 were combined and are shown in red while chains 3 and 4 are shown in blue. Overlaps of posterior distributions are thus shown in purple.

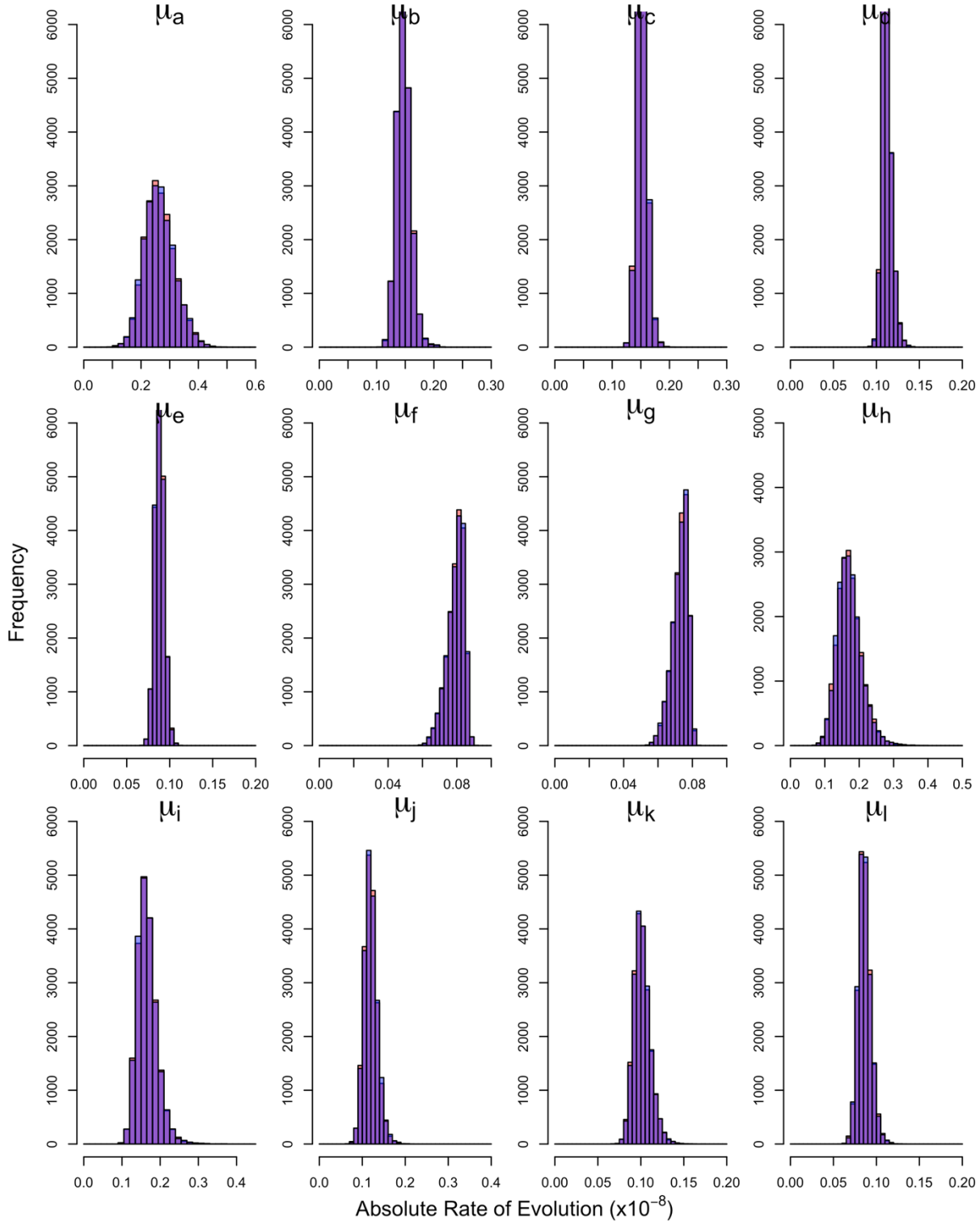

Figure S18 – Convergence of Posteriors for Replicate 10 without Partitioning by Substitution Type. Chains 1 and 2 were combined and are shown in red while chains 3 and 4 are shown in blue. Overlaps of posterior distributions are thus shown in purple.

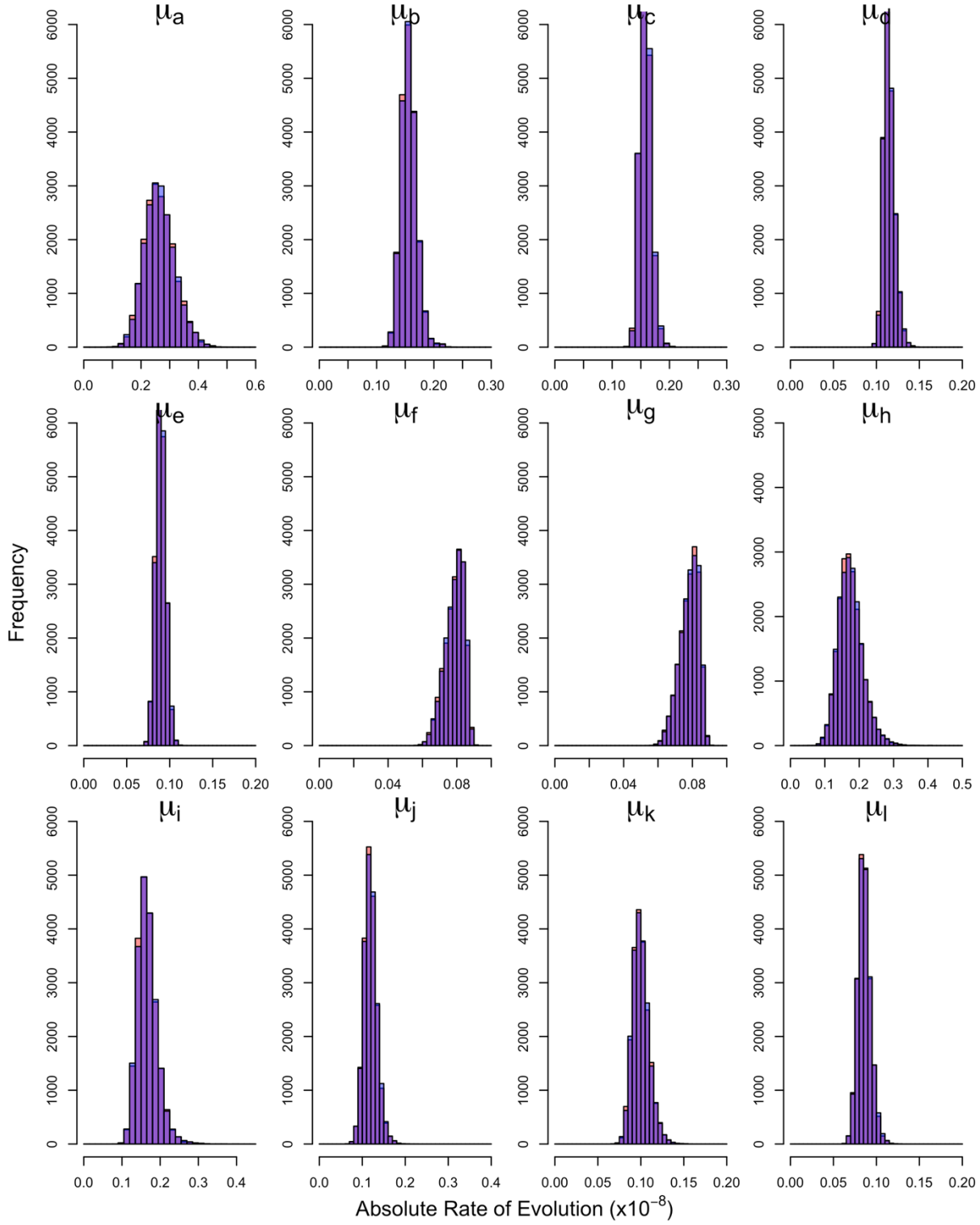

Figure S19 – Convergence of Node Heights Across Replicates. Points are median divergence times and lines are 95% HPD intervals. Substitution rates are from MCMCTREE analyses not partitioned by substitution type.

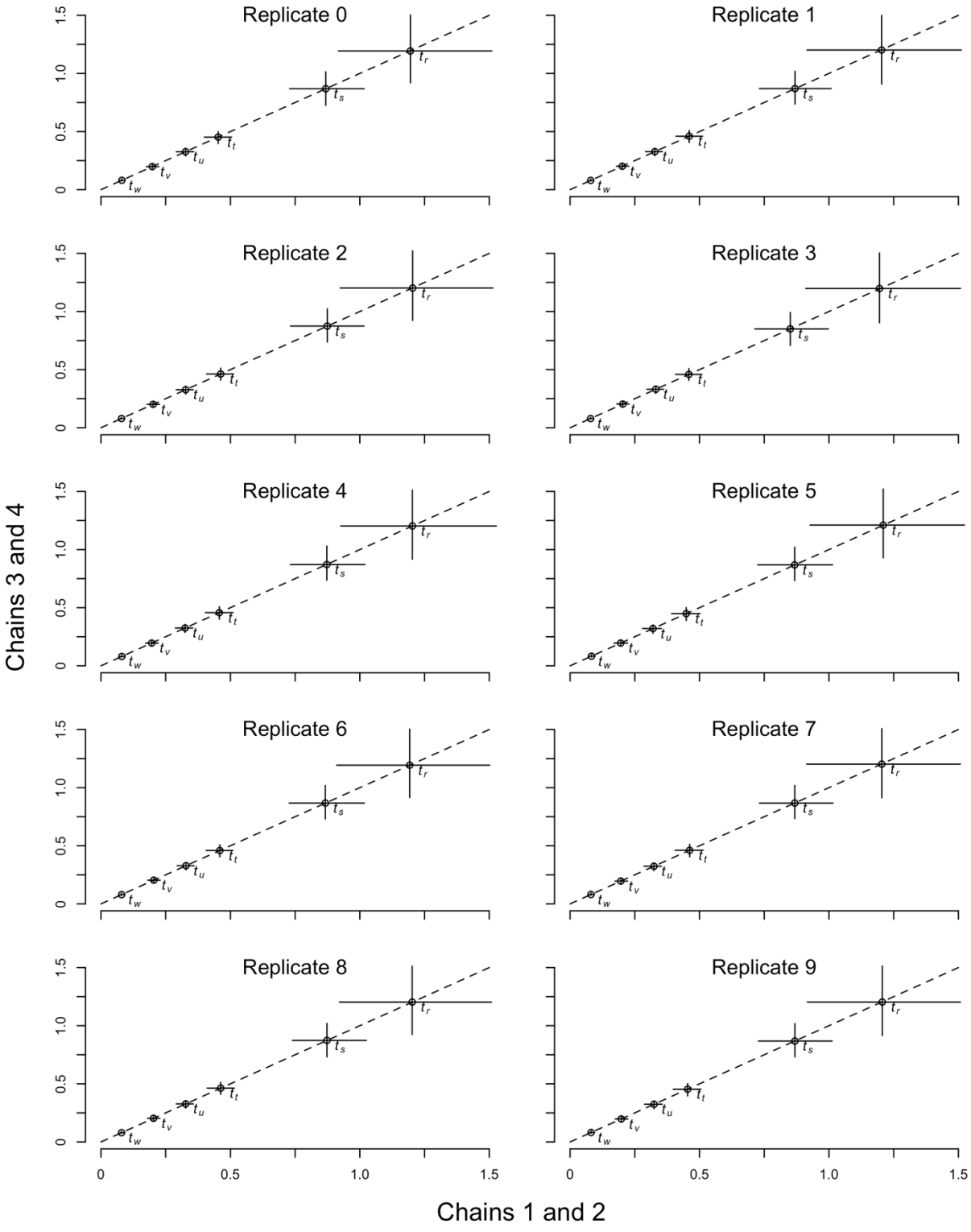

Figure S20 – Absolute Rates of Evolution for Tip Branches Across Replicates. Bar heights are mean rates and lines are 95% HPD intervals. Substitution rates are from MCMCTREE analyses not partitioned by substitution type.

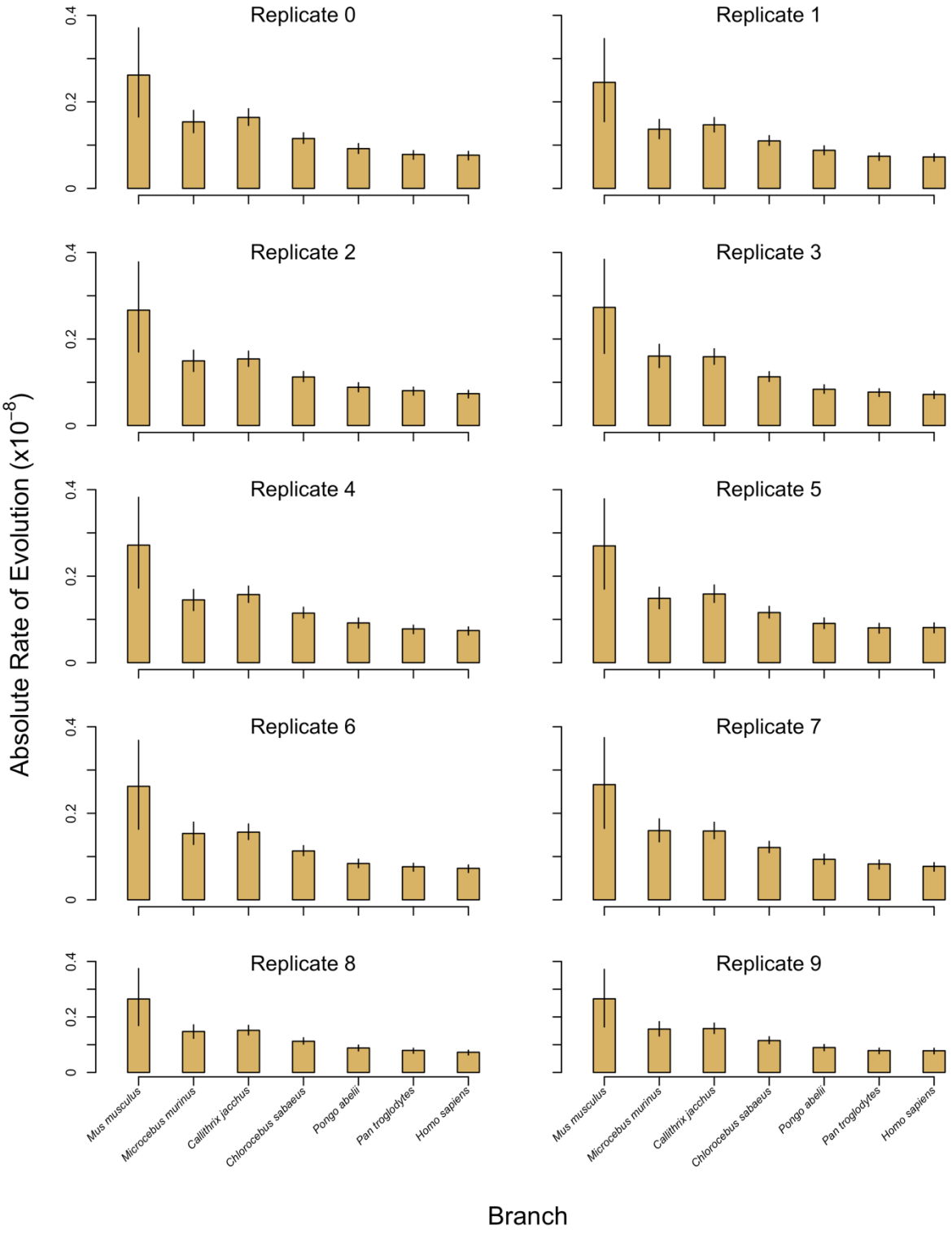

Figure S21 – Convergence of Posteriors for Replicate 1 with Partitioning by Substitution Type. Groups are defined in Table S2. Chain 1 is shown in red and chain 2 is blue. Overlap of posterior distributions are thus shown in purple.

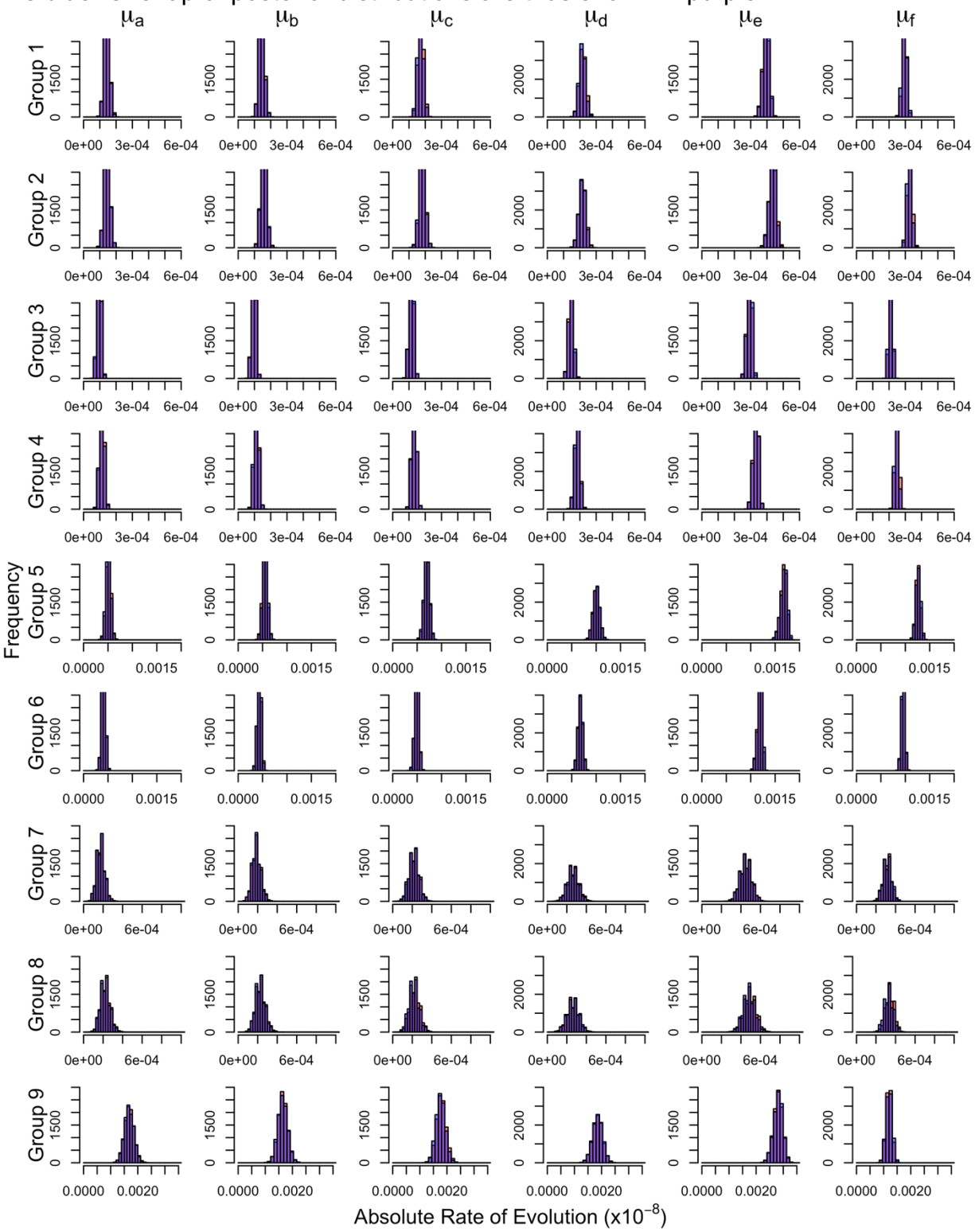

Figure S22 – Convergence of Posteriors for Replicate 2 with Partitioning by Substitution Type. Groups are defined in Table S2. Chain 1 is shown in red and chain 2 is blue. Overlap of posterior distributions are thus shown in purple.

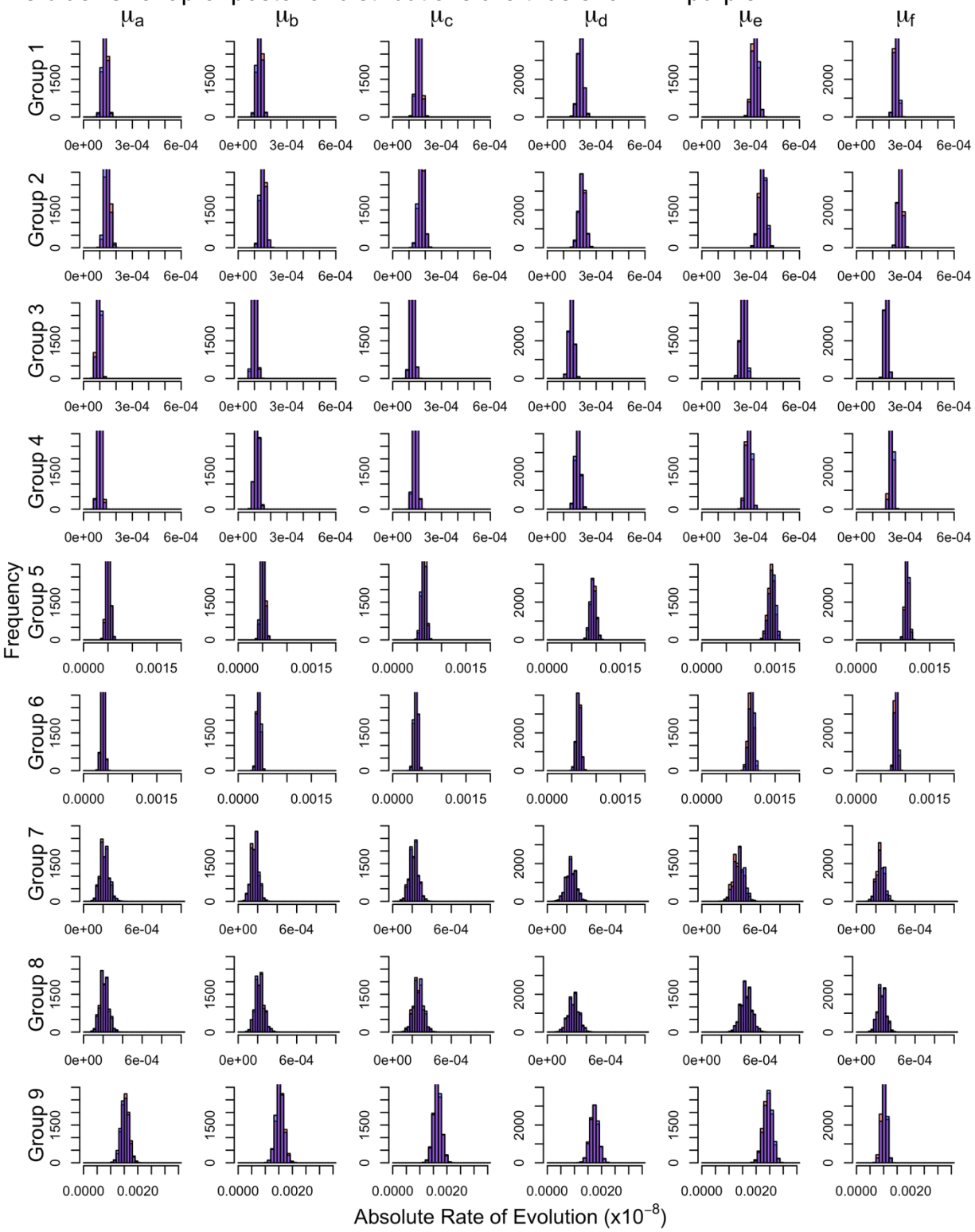

Figure S23 – Convergence of Posteriors for Replicate 3 with Partitioning by Substitution Type. Groups are defined in Table S2. Chain 1 is shown in red and chain 2 is blue. Overlap of posterior distributions are thus shown in purple.

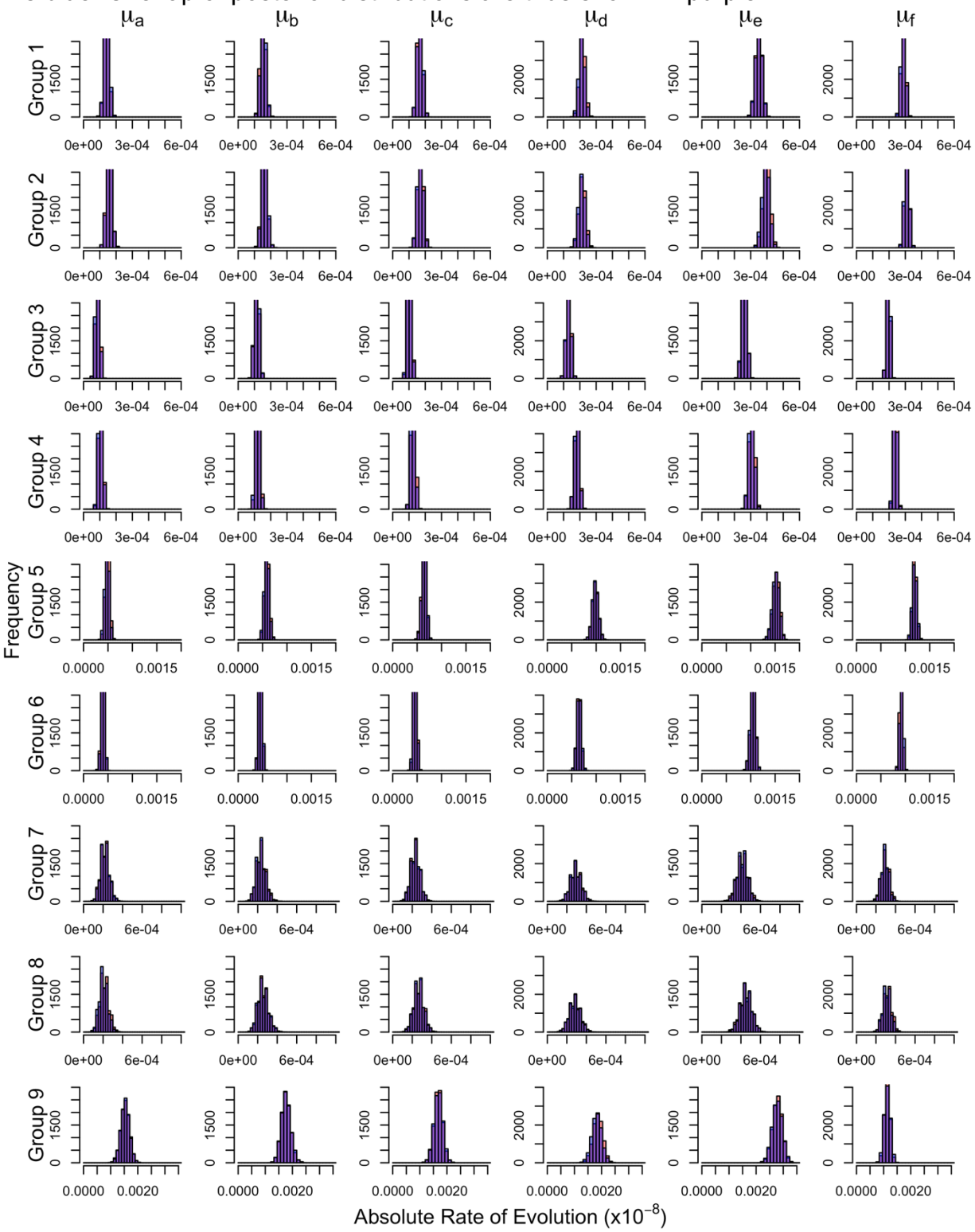

Figure S24 – Convergence of Posteriors for Replicate 4 with Partitioning by Substitution Type. Groups are defined in Table S2. Chain 1 is shown in red and chain 2 is blue. Overlap of posterior distributions are thus shown in purple.

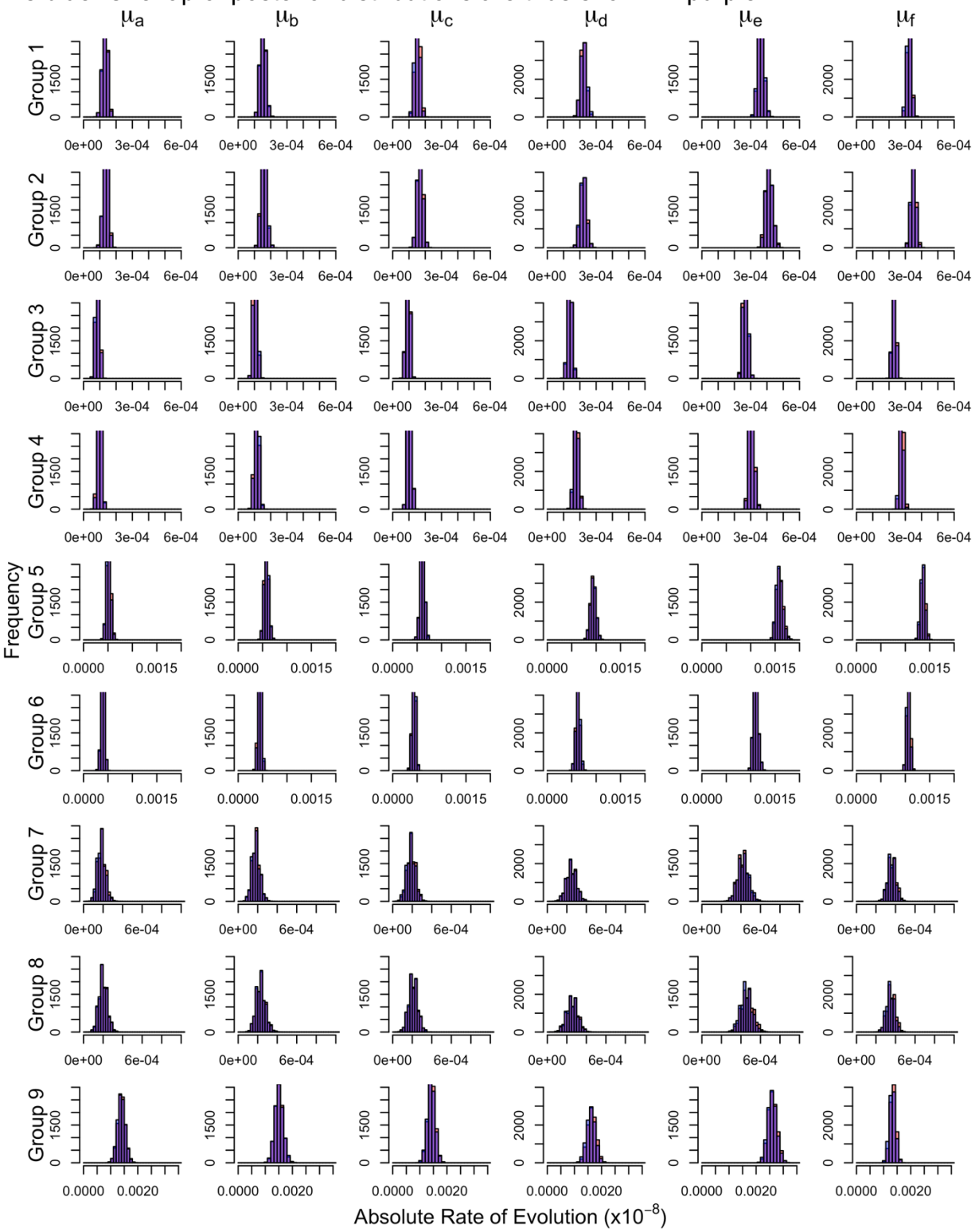

Figure S25 – Convergence of Posteriors for Replicate 5 with Partitioning by Substitution Type. Groups are defined in Table S2. Chain 1 is shown in red and chain 2 is blue. Overlap of posterior distributions are thus shown in purple.

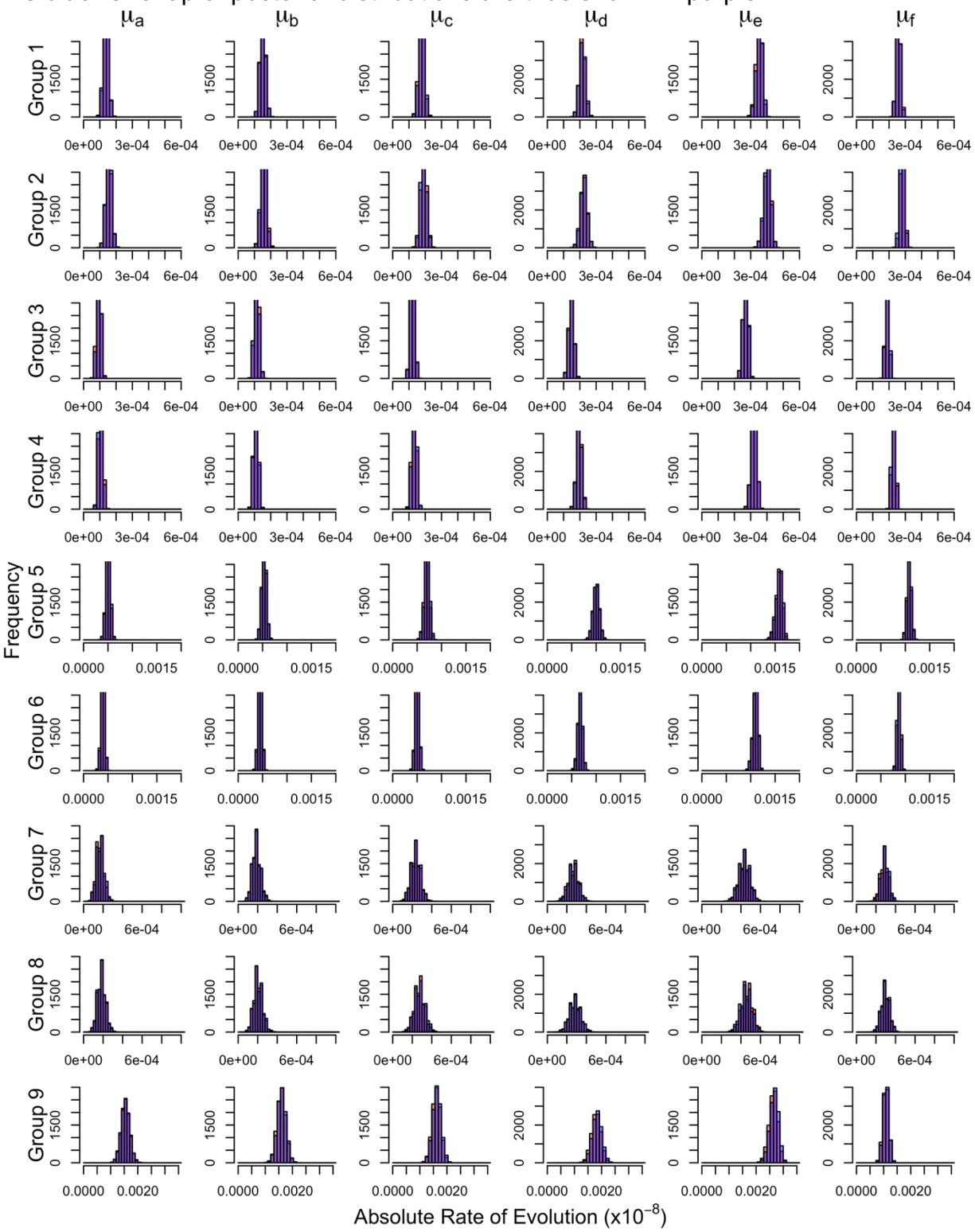

Figure S26 – Convergence of Posteriors for Replicate 6 with Partitioning by Substitution Type. Groups are defined in Table S2. Chain 1 is shown in red and chain 2 is blue. Overlap of posterior distributions are thus shown in purple.

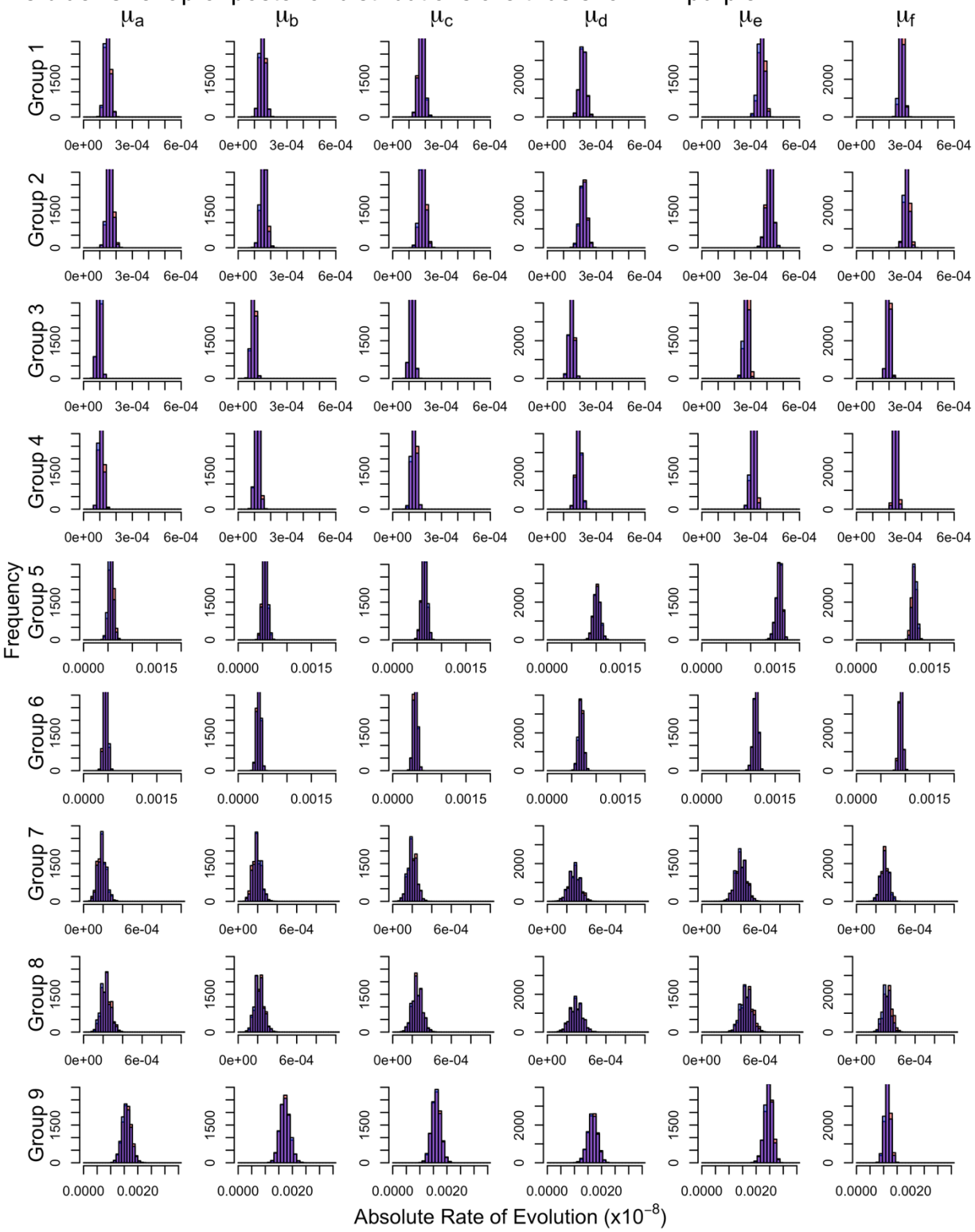

Figure S27 – Convergence of Posteriors for Replicate 7 with Partitioning by Substitution Type. Groups are defined in Table S2. Chain 1 is shown in red and chain 2 is blue. Overlap of posterior distributions are thus shown in purple.

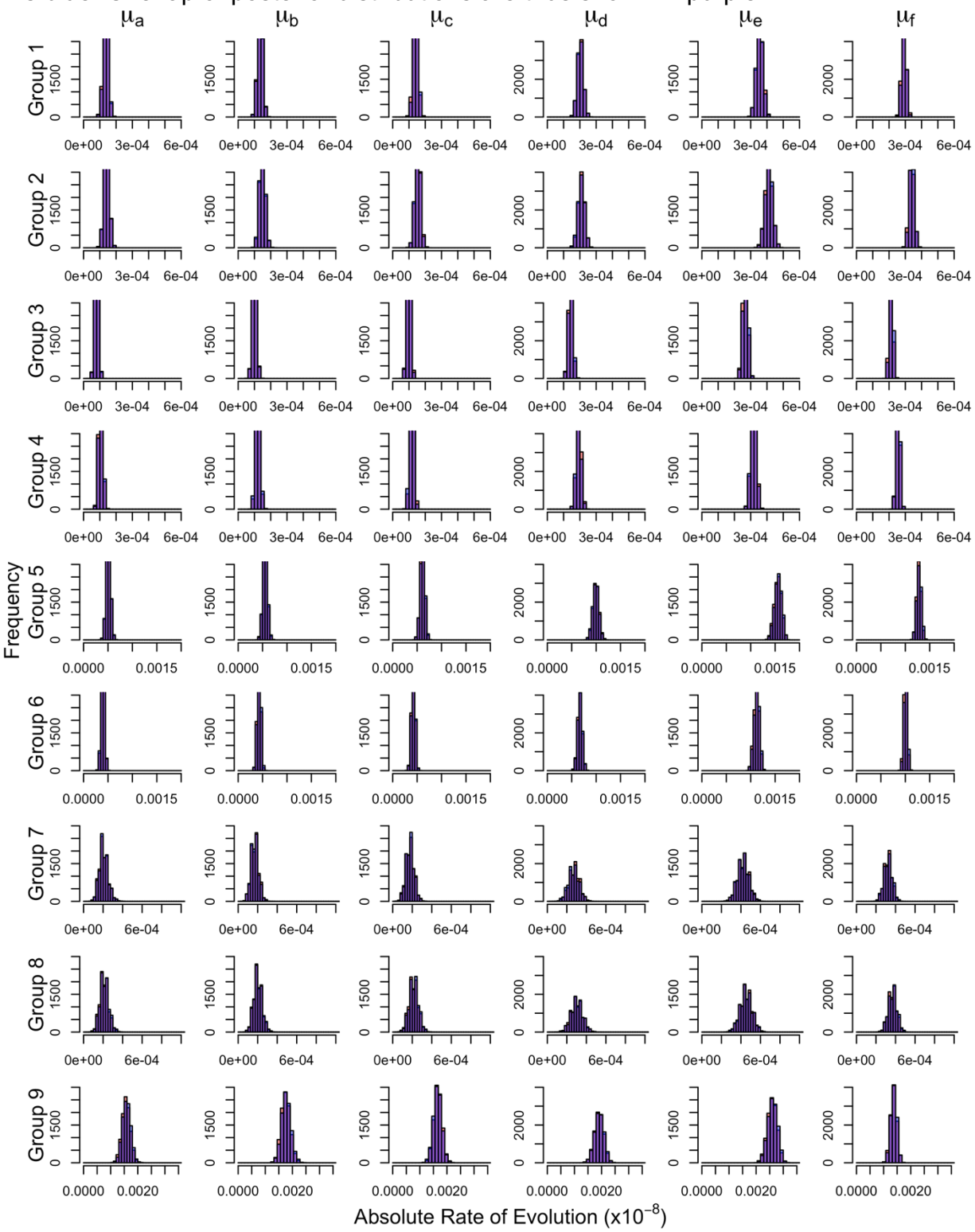

Figure S28 – Convergence of Posteriors for Replicate 8 with Partitioning by Substitution Type. Groups are defined in Table S2. Chain 1 is shown in red and chain 2 is blue. Overlap of posterior distributions are thus shown in purple.

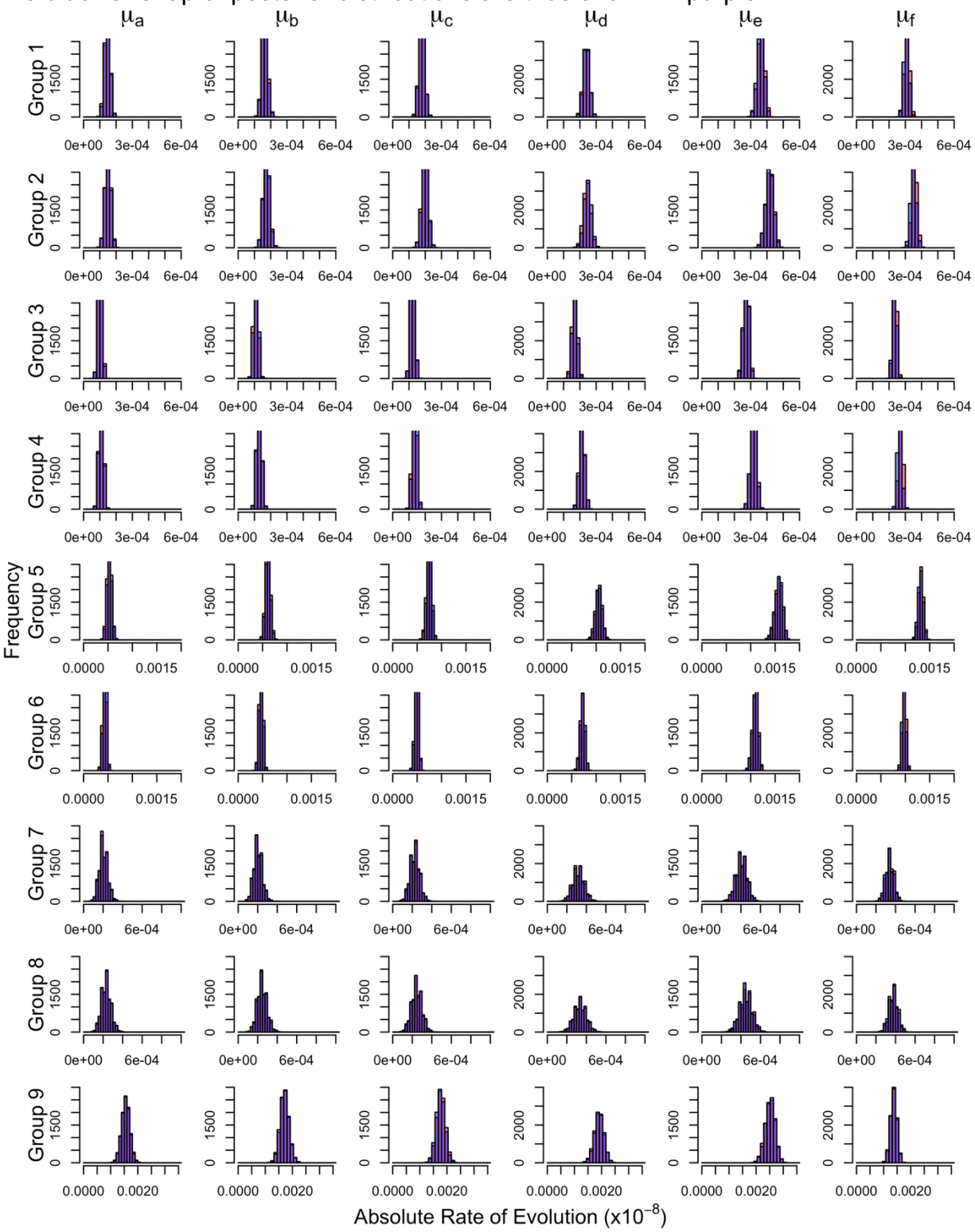

Figure S29 – Convergence of Posteriors for Replicate 9 with Partitioning by Substitution Type. Groups are defined in Table S2. Chain 1 is shown in red and chain 2 is blue. Overlap of posterior distributions are thus shown in purple.

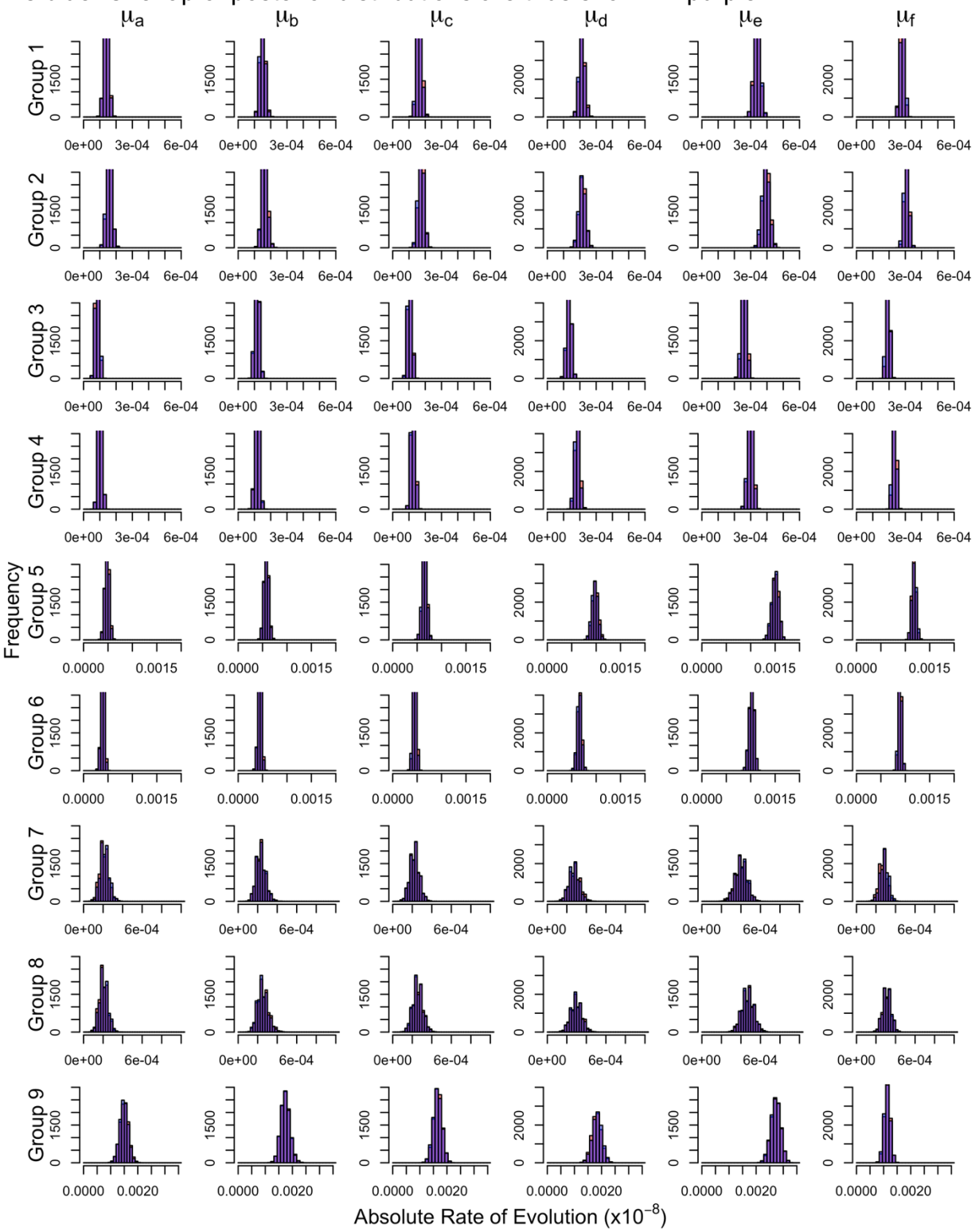

Figure S30 – Convergence of Posteriors for Replicate 10 with Partitioning by Substitution Type. Groups are defined in Table S2. Chain 1 is shown in red and chain 2 is blue. Overlap of posterior distributions are thus shown in purple.

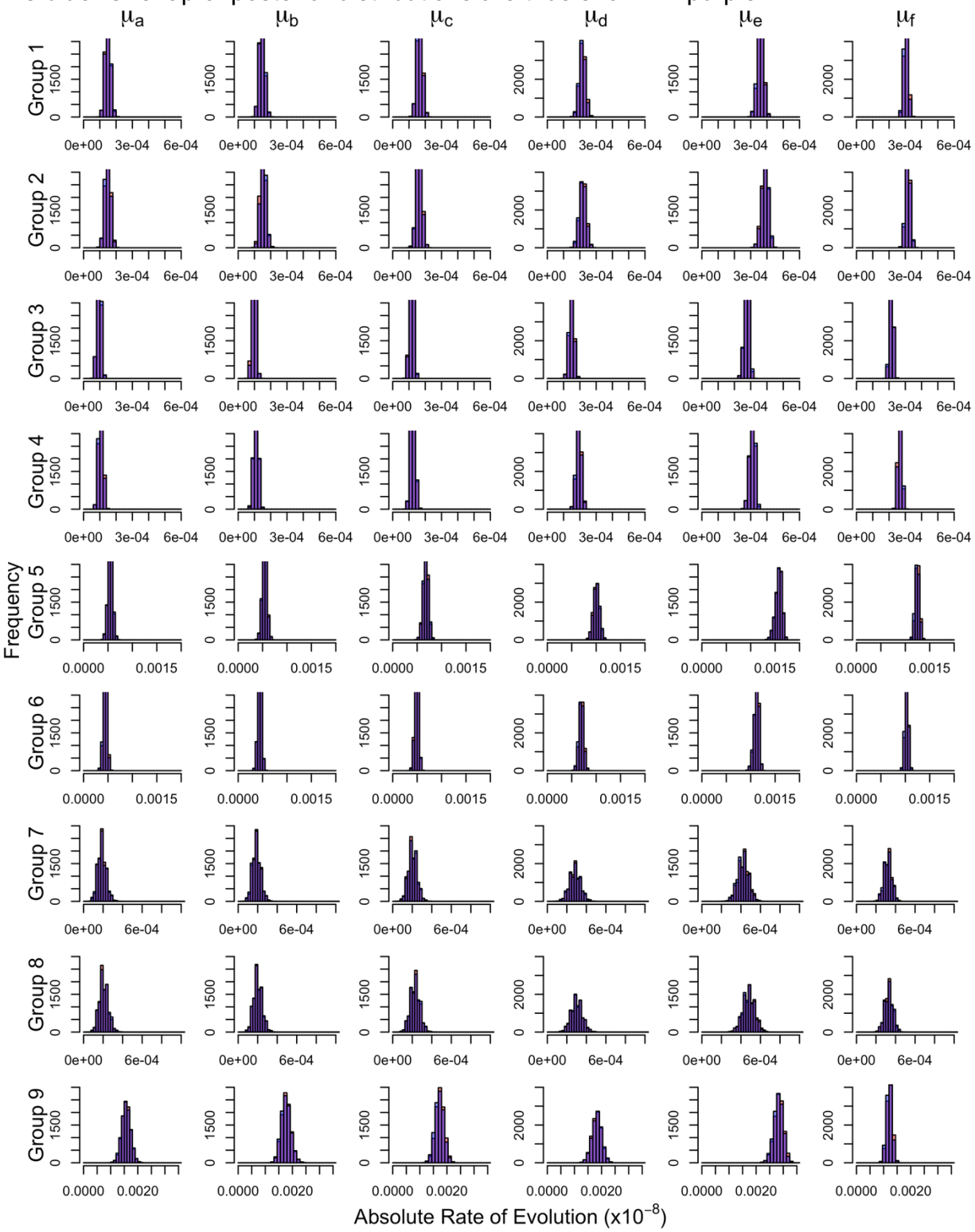

Figure S31 – Context-Dependent Absolute Rates of Evolution for Tip Branches for Replicate 1. Groups 1-6 are non-CpG sites and groups 7-9 are CpG sites. Bar heights are mean rates and lines are 95% HPD intervals.

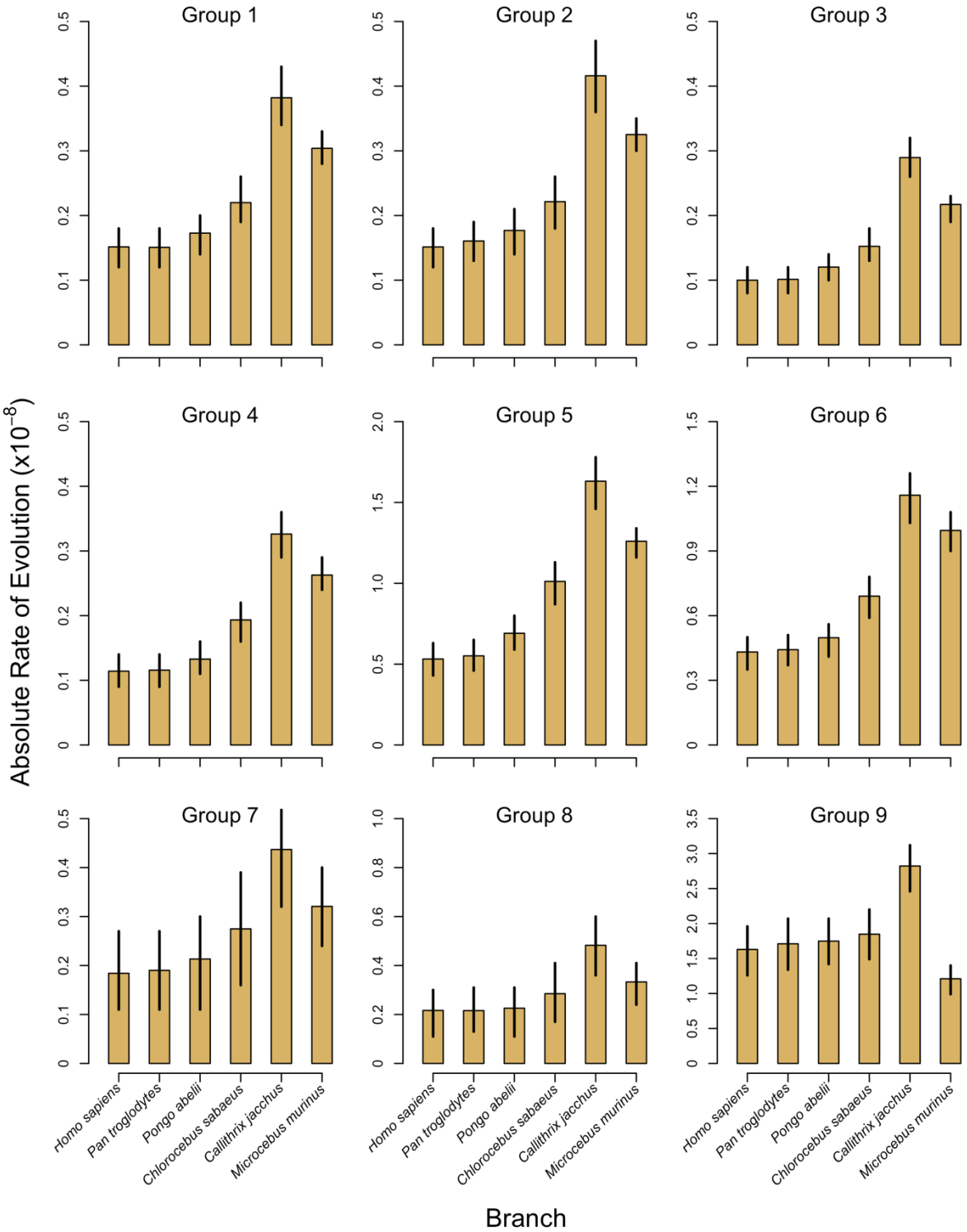

Figure S32 – Context-Dependent Absolute Rates of Evolution for Tip Branches for Replicate 2. Groups 1-6 are non-CpG sites and groups 7-9 are CpG sites. Bar heights are mean rates and lines are 95% HPD intervals.

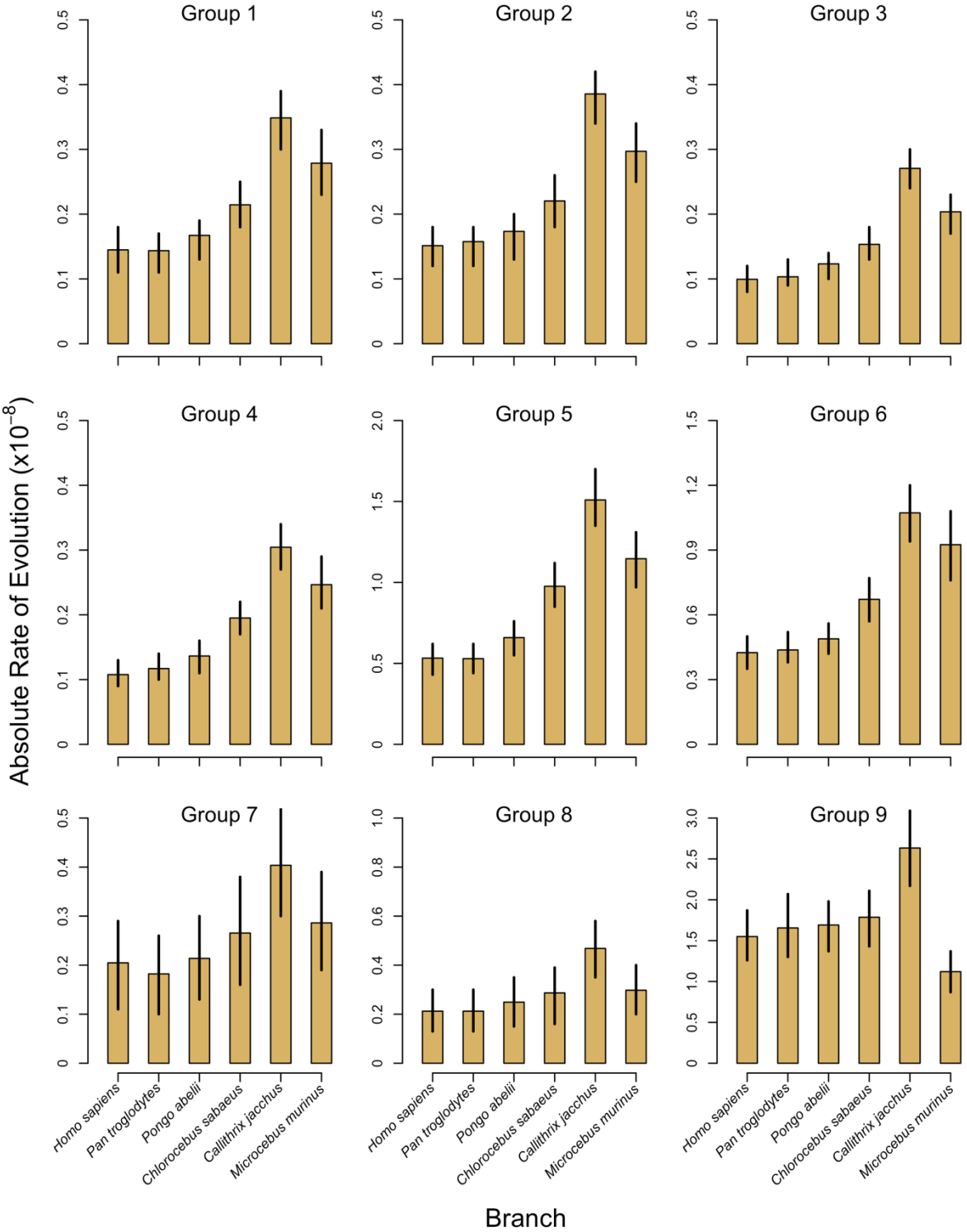

Figure S33 – Context-Dependent Absolute Rates of Evolution for Tip Branches for Replicate 3. Groups 1-6 are non-CpG sites and groups 7-9 are CpG sites. Bar heights are mean rates and lines are 95% HPD intervals.

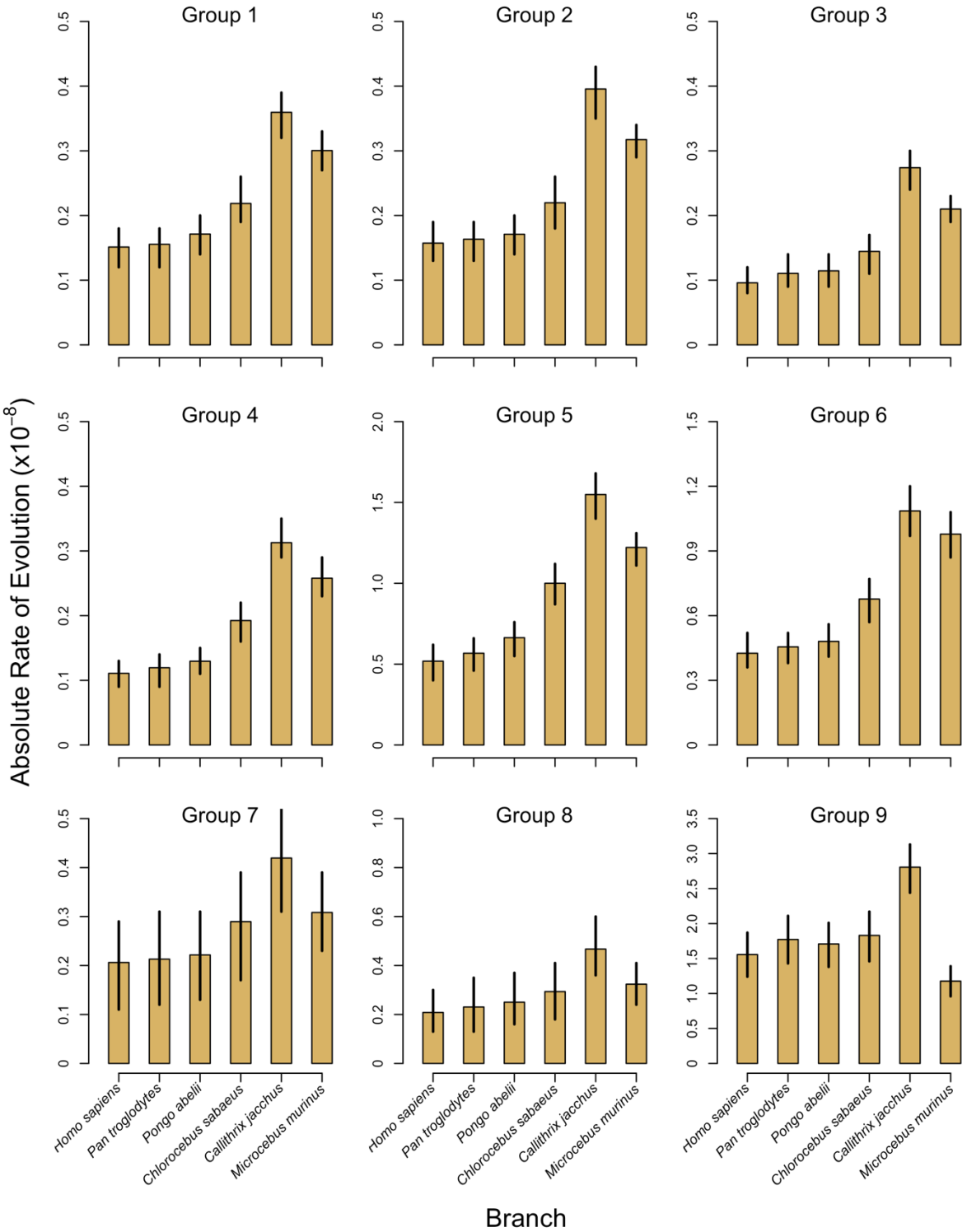

Figure S34 – Context-Dependent Absolute Rates of Evolution for Tip Branches for Replicate 4. Groups 1-6 are non-CpG sites and groups 7-9 are CpG sites. Bar heights are mean rates and lines are 95% HPD intervals.

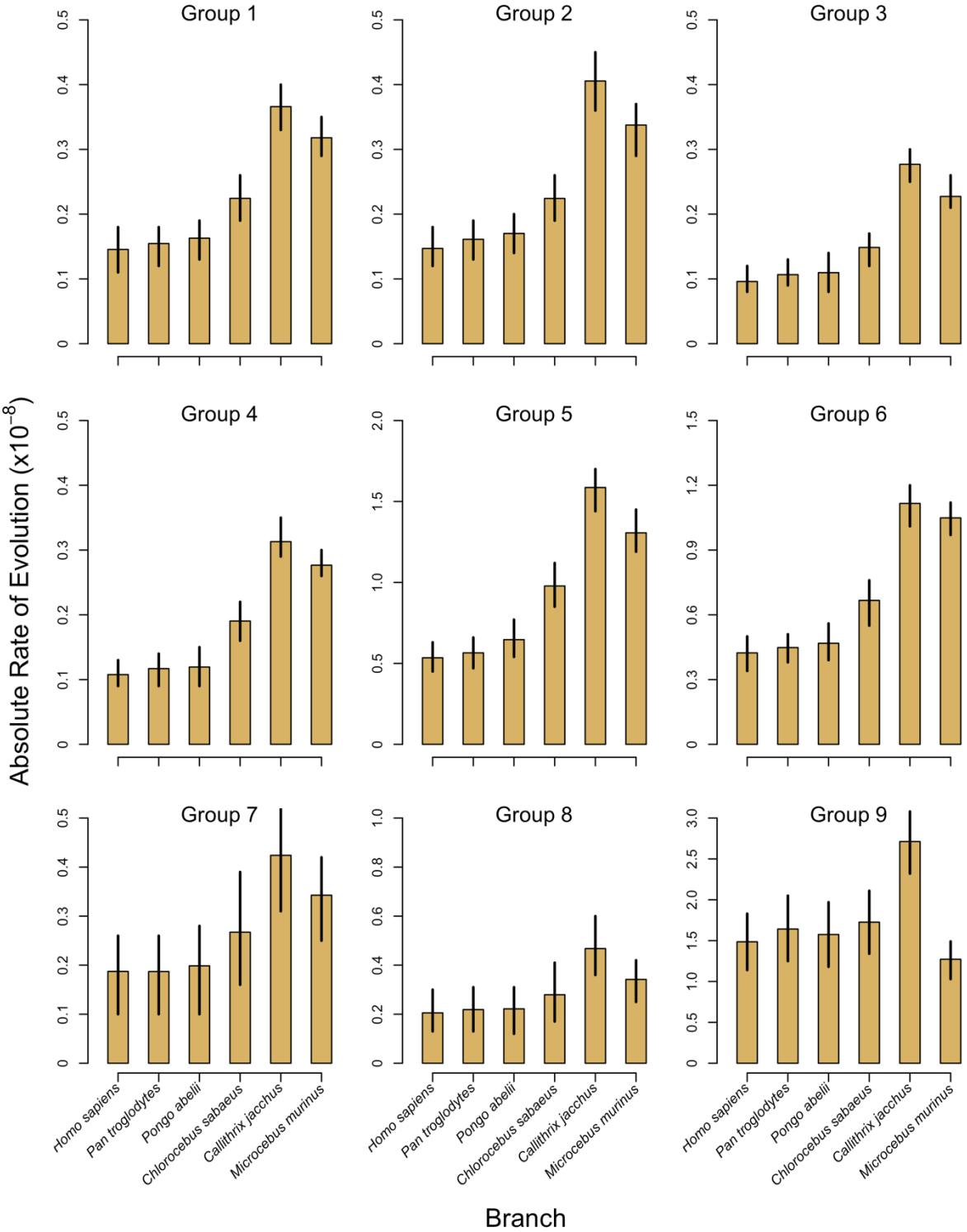

Figure S35 – Context-Dependent Absolute Rates of Evolution for Tip Branches for Replicate 5. Groups 1-6 are non-CpG sites and groups 7-9 are CpG sites. Bar heights are mean rates and lines are 95% HPD intervals.

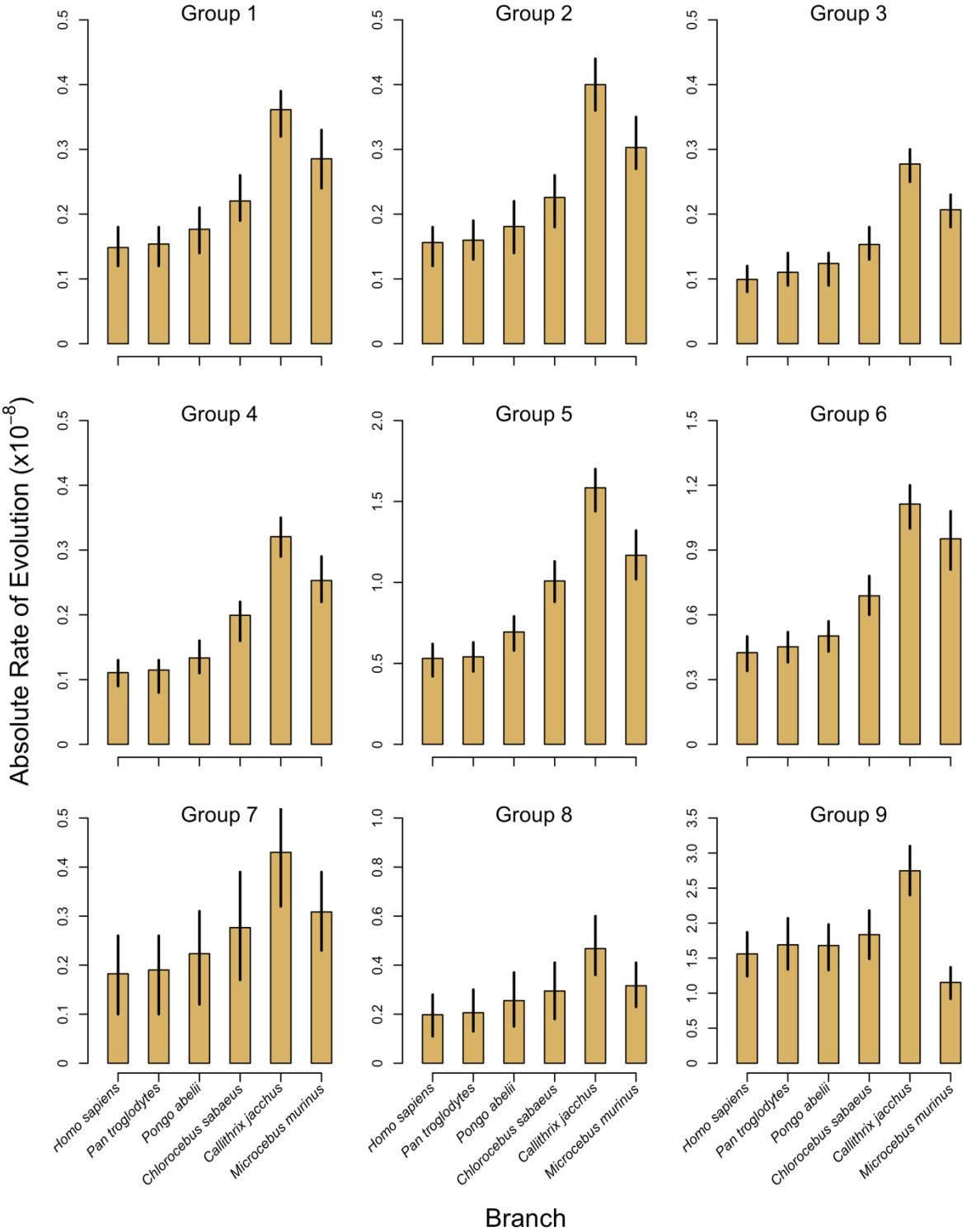

Figure S36 – Context-Dependent Absolute Rates of Evolution for Tip Branches for Replicate 6. Groups 1-6 are non-CpG sites and groups 7-9 are CpG sites. Bar heights are mean rates and lines are 95% HPD intervals.

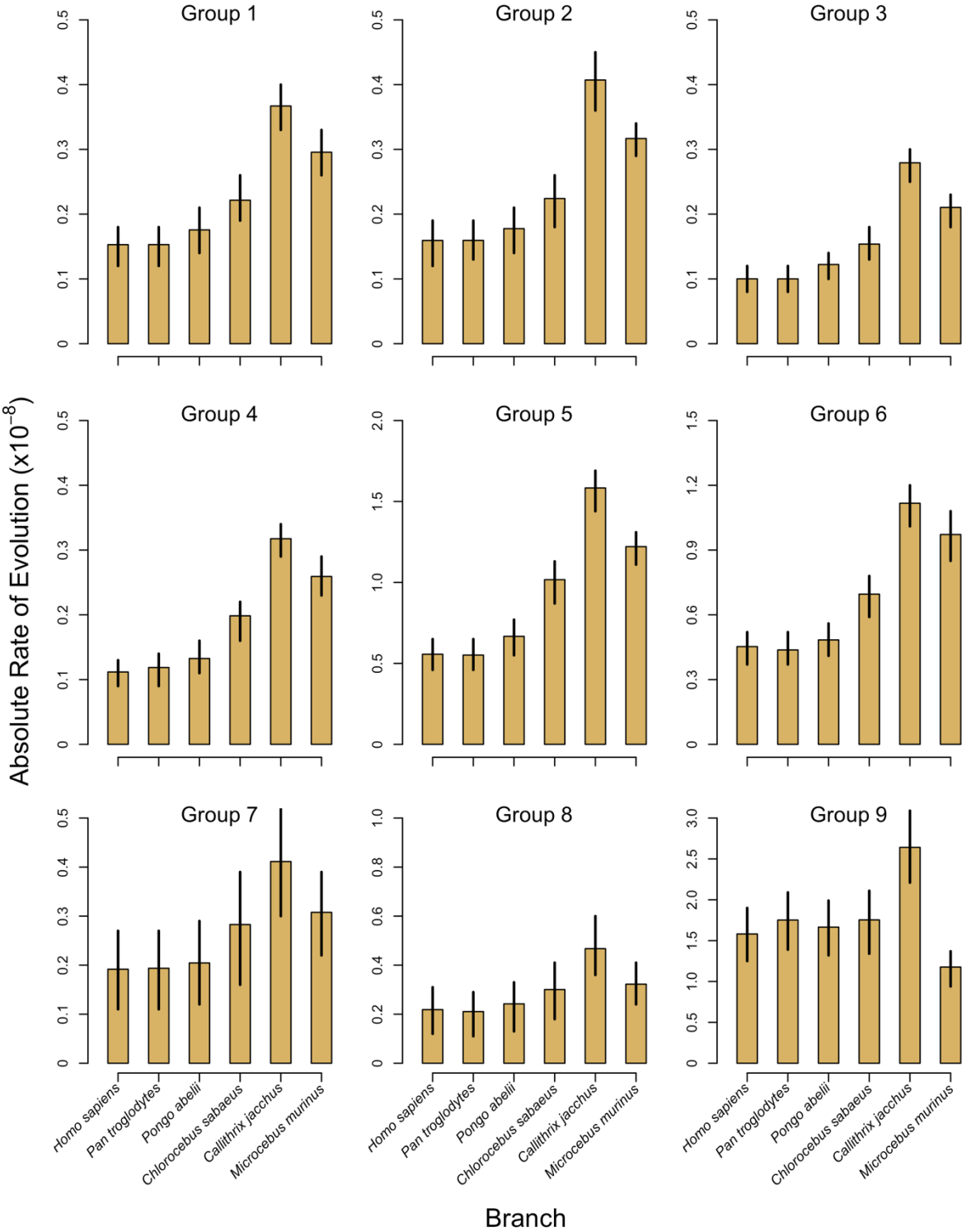

Figure S37 – Context-Dependent Absolute Rates of Evolution for Tip Branches for Replicate 7. Groups 1-6 are non-CpG sites and groups 7-9 are CpG sites. Bar heights are mean rates and lines are 95% HPD intervals.

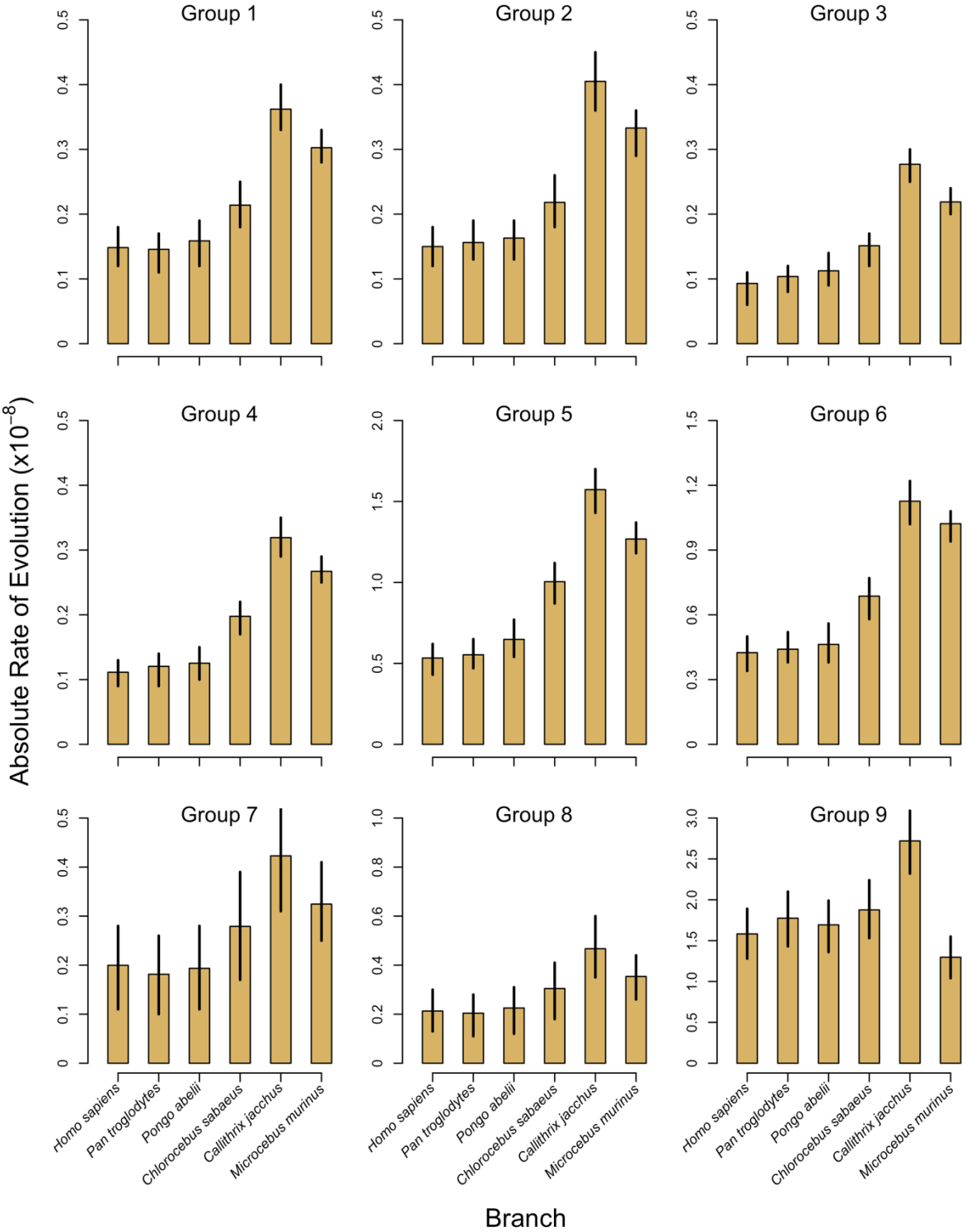

Figure S38 – Context-Dependent Absolute Rates of Evolution for Tip Branches for Replicate 8. Groups 1-6 are non-CpG sites and groups 7-9 are CpG sites. Bar heights are mean rates and lines are 95% HPD intervals.

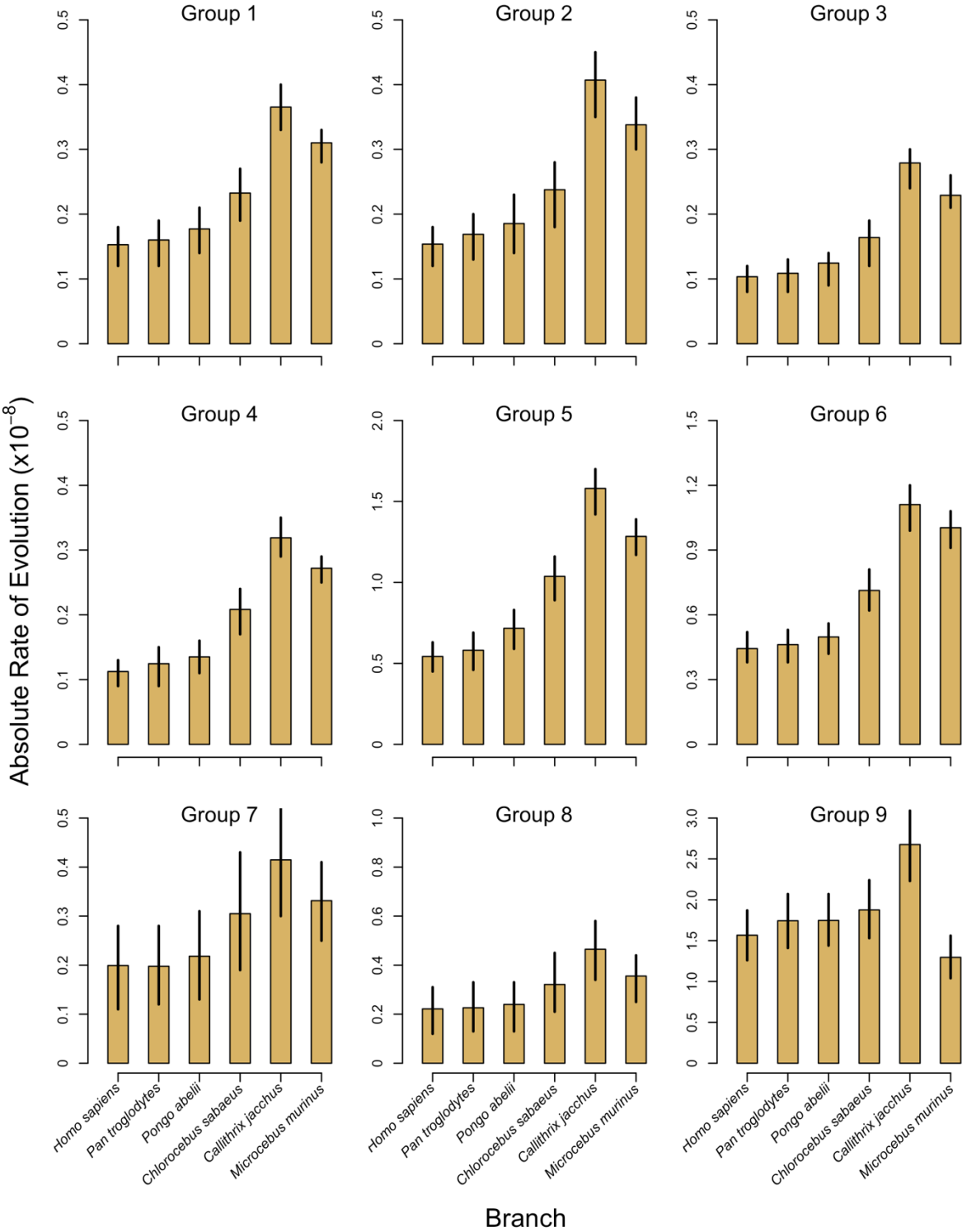

Figure S39 – Context-Dependent Absolute Rates of Evolution for Tip Branches for Replicate 9. Groups 1-6 are non-CpG sites and groups 7-9 are CpG sites. Bar heights are mean rates and lines are 95% HPD intervals.

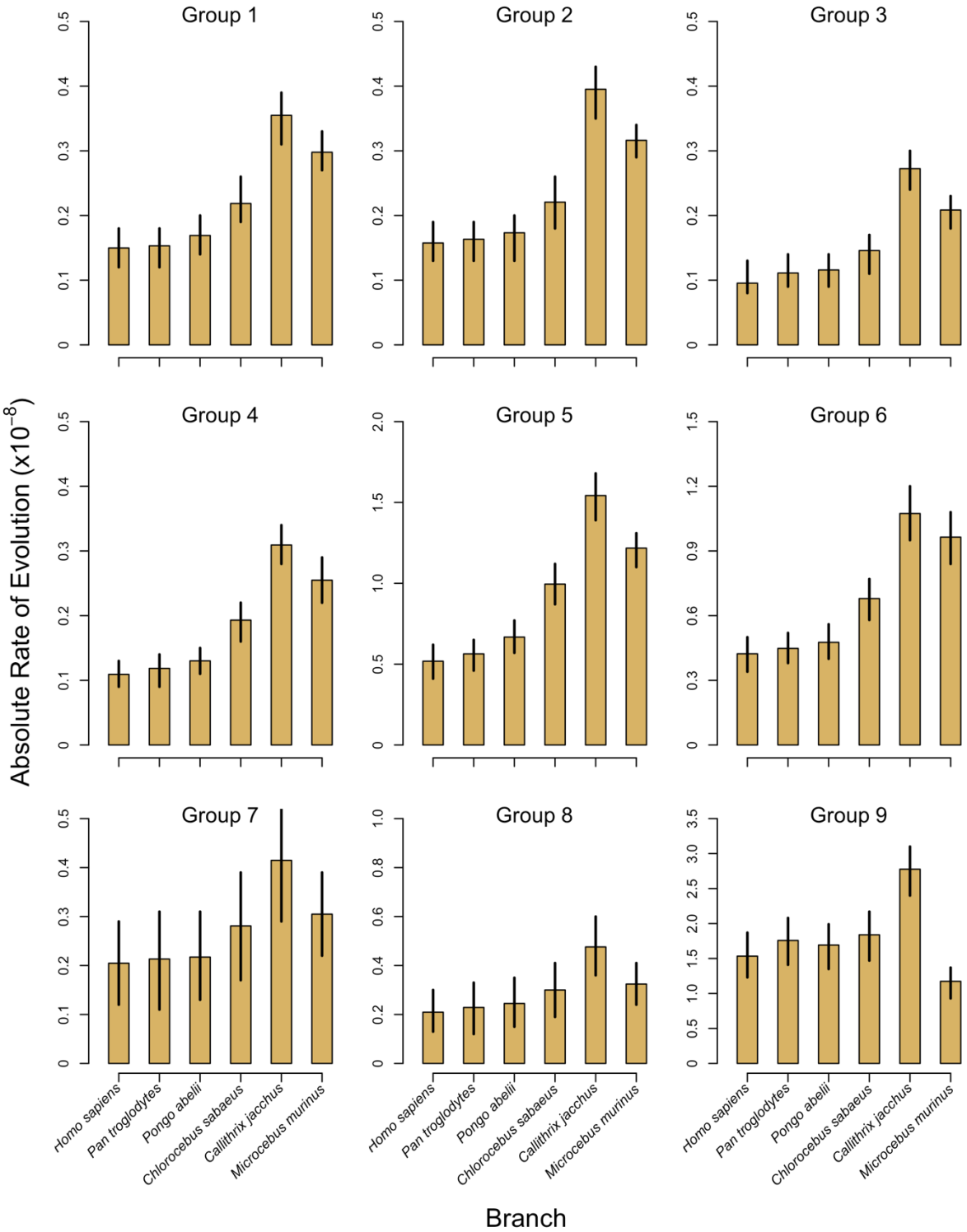

Figure S40 – Context-Dependent Absolute Rates of Evolution for Tip Branches for Replicate 10. Groups 1-6 are non-CpG sites and groups 7-9 are CpG sites. Bar heights are mean rates and lines are 95% HPD intervals.

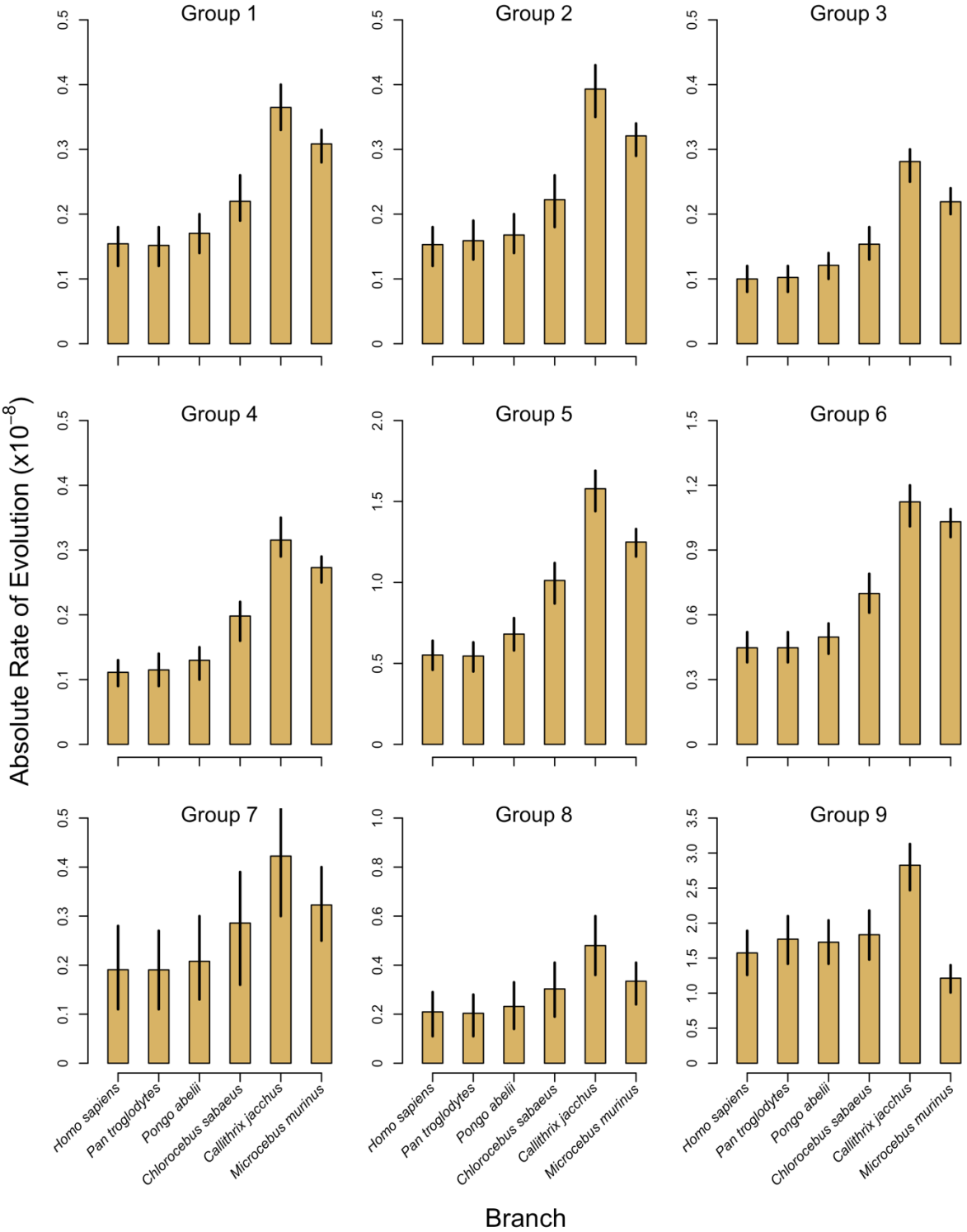

Supplementary Tables

Table S1 – Fossil Calibrations for Clock Model Analyses.

Node	MCMCTREE	Description	MULTIDIVTIME	Description
t_w	B(0.075,0.10,0.01,0.20)	Soft lower and upper bounds of 7.5 and 10 MYA	(7.5,10.0)	Hard lower and upper bounds of 7.5 and 10 MYA
t_v	B(0.112,0.28,0.01,0.10)	Soft lower and upper bounds of 11.2 and 28 MYA	(11.2,28.0)	Hard lower and upper bounds of 11.2 and 28 MYA
t_u	B(0.25,0.337,0.01,0.10)	Soft lower and upper bounds of 25 and 33.7 MYA	(25,33.7)	Hard lower and upper bounds of 25 and 33.7 MYA
t_t	ST(0.4754,0.0632,0.98,22.85)	Skew T with a minimum near 47.5 MYA	(41,62.1)	Hard lower and upper bounds of 41 and 62.1 MYA
t_s	S2N(0.698,0.65,0.0365,-3400,0.6502,0.1375,11409)	Mixture of two skew Normal Distributions that places divergence of Strepsirrhini and Haplorrhini before KT boundary	89.1	Ingroup root node constrained to 89.1 based on MCMCTREE posteriors. Allowed only a small amount of variation with SD of 0.2.
t_r	G(36,36.9)	A vague root calibration with mean of 97.5 MYA	NA†	NA†

† MULTIDIVTIME only allows for ingroup root node calibration while constraining the branches subtending t_s and t_r to the same rate

Table S2 – Substitution Types for MULTIDIVTIME Analyses.

Group	Substitutions	Description	Context
1	G>C and C>G	strong-to-strong transversions	non-CpG
2	G>T and C>A	strong-to-weak transversions	non-CpG
3	T>A and A>T	weak-to-weak transversions	non-CpG
4	T>G and A>C	weak-to-strong transversions	non-CpG
5	G>A and C>T	strong-to-weak transitions	non-CpG
6	A>G and T>C	weak-to-strong transitions	non-CpG
7	G>C and C>G	strong-to-strong transversions	CpG
8	G>T and C>A	strong-to-weak transversions	CpG
9	G>A and C>T	strong-to-weak transitions	CpG

Table S3. Mutation rates and substitution rates (calculated per year and per generation. Mutation rate references are in Table 1 and substitution rates are taken from dos Reis et al. (2018).

Species	Per-Year Rate Substitution			Per-Generation Rate Mutation			Per-Generation Rate Substitution			Generation Time (years)	Paternal Generation Time (years)	Generation Time Citation
	Mean	Lower	Upper	Mean	Lower	Upper	Mean	Lower	Upper			
Chlorocebus sabaeus	8.48E-10	4.76E-10	1.25E-09	9.4E-09	NA	NA	7.20E-09	4.04E-09	1.06E-08	8.5[†]	NA	Warren et al. 2015
Pan troglodytes	7.13E-10	4.18E-10	1.06E-09	1.27E-08	9.5E-09	1.70E-08	1.25E-08	7.35E-09	8.97E-09	17.58	19.27	Besenbacher et al. 2019
Homo sapiens	7.54E-10	5.44E-10	9.80E-10	1.20E-08	6.7E-09	1.70E-08	2.27E-08	1.64E-08	8.33E-09	30.1	31.63	Jonsson et al. 2017
Gorilla gorilla	8.49E-10	3.24E-10	1.50E-09	1.125E-08	9.1E-09	1.60E-08	1.48E-08	5.66E-09	1.28E-08	17.5	13.5	Besenbacher et al. 2019
Pongo abelii	3.56E-10	1.73E-10	5.70E-10	1.66E-08	1.30E-08	2.20E-08	8.18E-09	3.97E-09	4.85E-09	23	31	Besenbacher et al. 2019
Aotus nancymaae	5.40E-10	2.98E-10	8.17E-10	8.1E-09	8.1E-09	8.1E-09	3.56E-09	1.96E-09	6.94E-09	6.59	5.55	Thomas et al. 2018
Microcebus murinus	1.72E-09	9.51E-10	2.56E-09	1.74E-08	1.5E-08	2.1E-08	5.16E-09	2.85E-09	2.18E-08	3	4.55	This Study
Macaca mulatta	6.94E-10	4.16E-10	9.92E-10	5.80E-09	NA	NA	5.21E-09	3.12E-09	8.43E-09	7.5	7.8	Wang et al. 2020
Papio anubis	5.97E-10	3.36E-10	8.92E-10	5.70E-09	5.10E-09	6.40E-09	5.85E-09	3.29E-09	7.58E-09	9.8	10.27	Wu et al. 2019

Table S4. Ancestral effective population size (N_e) and estimated divergence times from BPP. Node labels corresponding to Figure 6. Means and 95% confidence intervals are given for effective population size and divergence time estimates. The previous analysis drew rates at random from a gamma distribution for each posterior sample, so confidence intervals are used again here for consistency.

Mutation Rate	node	N_e x10^3	95% CI	Divergence Time (ka)	95% CI
1.52x10^{-8} (This Study)	E	171	141, 202	304	219, 396
	D	11.9	5.90, 16.2	174	128, 223
	A	44.0	28.7, 59.1	29.1	5.40, 60.9
	C	2.22	1.31, 2.97	161	118, 207
	B	49.2	34.4, 64.6	9.76	0.33, 28.7
0.87x10^{-8} (Yoder et al. 2016)	E	307	200, 429	546	314, 794
	D	21.5	8.66, 34.6	313	190, 455
	A	79.0	43.5, 119	52.4	7.19, 112
	C	3.98	1.91, 6.13	290	175, 422
	B	88.4	51.0, 130	17.6	0.44, 52.1

Supplementary References

Besenbacher S, Hvilsom C, Marques-Bonet T, Mailund T, Schierup MH. 2019. Author Correction: Direct estimation of mutations in great apes reconciles phylogenetic dating. Nature Ecology & Evolution 3:859-859.

dos Reis M, Gunnell GF, Barba-Montoya J, Wilkins A, Yang Z, Yoder AD. 2018. Using Phylogenomic Data to Explore the Effects of Relaxed Clocks and Calibration Strategies on Divergence Time Estimation: Primates as a Test Case. Systematic Biology 67:594-615.

Jónsson H, Sulem P, Kehr B, Kristmundsdottir S, Zink F, Hjartarson E, Hardarson MT, Hjorleifsson KE, Eggertsson HP, Gudjonsson SA, et al. 2017. Parental influence on human germline *de novo* mutations in 1,548 trios from Iceland. Nature 549:519.

Thomas GWC, Wang RJ, Puri A, Harris RA, Raveendran M, Hughes DST, Murali SC, Williams LE, Doddapaneni H, Muzny DM, et al. 2018. Reproductive Longevity Predicts Mutation Rates in Primates. Current Biology 28:3193-3197.e3195.

Warren WC, Jasinska AJ, García-Pérez R, Svardal H, Tomlinson C, Rocchi M, Archidiacono N, Capozzi O, Minx P, Montague MJ, et al. 2015. The genome of the vervet (*Chlorocebus aethiops sabaeus*). Genome Res. 2512:1921-1933.

Wu FL, Strand A, Ober C, Wall JD, Moorjani P, Przeworski M (2019). A comparison of humans and baboons suggests germline mutation rates do not track cell divisions. *bioRxiv* doi: https://doi.org/10.1101/844910.

Wang RJ, Thomas GWC, Raveendran M, Harris RA, Doddapaneni H, Muzny DM *et al* (2020). Paternal age in rhesus macaques is positively associated with germline mutation accumulation but not with measures of offspring sociability. *Genome Res* **30**(6)**:** 826-834.

Yoder AD, Campbell CR, Blanco MB, dos Reis M, Ganzhorn JU, Goodman SM, Hunnicutt KE, Larsen PA, Kappeler PM, Rasoloarison RM, et al. 2016. Geogenetic patterns in mouse lemurs (genus *Microcebus*) reveal the ghosts of Madagascar's forests past. Proc Natl Acad Sci USA. 113:8049-8056.